Role of Vascular Smooth Muscle Cell PiT-2 in Basal Ganglia Calcification

Jia Jun Chia

A thesis

submitted in partial fulfillment of the

requirements for the degree of

Master of Science in Bioengineering

University of Washington

2016

Committee:

Cecilia M. Giachelli

Marta Scatena

Program Authorized to Offer Degree:

Bioengineering

University of Washington

Abstract

Role of Vascular Smooth Muscle Cell PiT-2 in Basal Ganglia Calcification

Jia Jun Chia

Chair of the Supervisory Committee:
Professor Cecilia M. Giachelli
Bioengineering

Idiopathic basal ganglia calcification (IBGC) is a rare neurodegenerative disorder that can be inherited in an autosomal dominant manner. The disease is characterized by bilateral calcium phosphate salt deposition primarily in the arterioles in the basal ganglia and thalamic region of the brain that result in symptoms such as vascular dementia, motor control disorders and strokes. However, there is currently no cure for IBGC. Recent genome studies have associated mutations in the gene that encodes a sodium-dependent phosphate (Pi) transporter, PiT-2, with approximately 50% of IBGC cases. PiT-2 is highly localized to vascular smooth muscle cells (VSMCs) in the cerebral vessels, and we hypothesized that PiT-2 in the VSMCs specifically plays a role in protecting VSMCs against calcification. In this research study, we developed an siRNA-based *in vitro* model in VSMCs to understand the etiology behind this disease. We observed a decrease in sodium-dependent Pi uptake levels but an increase in Pi-induced calcification following PiT-2 knockdown (KD), consistent with a protective role in

VSMCs. Using PiT-2 KD VSMCs, we also investigated several mechanisms of vascular calcification and discovered that PiT-2 may normally inhibit cell death and maintain the level of calcification inhibitors. Based on previous studies showing that global PiT-2 haploinsufficient mice accurately recapitulated human BGC, an SM22α promoter-driven Cre knockout mouse model was developed for this study to investigate if PiT-2 in VSMCs were necessary for the inhibition of BGC. Characterization of the knockout mouse model showed that the deletion of PiT-2 in VSMCs is not sufficient to cause BGC, suggesting that VSMCs may not be the only cell type involved in the development of BGC. To our knowledge, this is the first mechanistic study investigating the role of VSMC PiT-2 in BGC, which is significant as it not only advances our understanding of the etiology underlying BGC, but also opens possibilities for developing therapeutics to target this disease.

Table of Contents

List of Figures iii

List of Tables iv

List of Abbreviations v

Introduction 1

Chapter 1. Background and Significance 3

1.1 IBGC 3
1.2 Sodium-dependent Pi transporters 5
1.3 VC 7
1.3.1 VSMCs 9
1.3.2 Failed anticalcific processes 10
1.3.3 OC differentiation 11
1.3.4 Cell death 12
1.3.5 ECM remodeling 12
1.3.6 Dysregulated mineral metabolism 13
1.4 Tissue-specific gene deletion 15

Chapter 2. Materials and Methods 17

2.1 Materials 17
2.1.1 Tissue culture reagents 17
2.1.2 Other reagents 17
2.1.3 Laboratory equipment 18
2.1.4 Software 18
2.2 Methods 19
2.2.1 VSMC isolation and culture 19
2.2.2 siRNA-mediated knockdown of PiT-2 20
2.2.3 Pi uptake assay 20
2.2.4 Calcification assay 20
2.2.5 PPi assay 21
2.2.6 Cell death assay 22
2.2.7 Gene Expression 22
2.2.7.1 qPCR 22
2.2.7.2 RNA-Seq 23
2.2.8 Protein expression 24
2.2.9 Generation of PiT-2 ΔSM mouse 24
2.2.10 Tissue characterization 25
2.2.10.1 DNA extraction from tissues 25
2.2.10.2 Genotyping of genomic DNA 26
2.2.10.3 Histological preparation of tissues 27

2.2.10.4 Alizarin Red S staining 27
2.2.10.5 SM22α immunofluorescence (IF) 27
2.2.11 Cisternal CSF collection and CSF Pi measurement 28
2.2.12 Statistics 28

Chapter 3. Results 29

3.1 PiT-2 haploinsufficiency results in basal ganglia calcification 29
3.1.1 PiT-2 haploinsufficient mice developed age-dependent BGC 29
3.1.2 BGC was associated with cerebral arterioles, specifically arteriolar VSMCs 30
3.1.3 PiT-2 was expressed in choroid plexus and ependyma, and required for regulation of CSF Pi levels 32
3.2 Role of PiT-2 in VSMCs *in vitro* 33
3.2.1 siRNA-mediated knockdown of PiT-2 in VSMCs enhanced Pi-induced calcification 33
3.2.2 Reduced secreted PPi levels not observed in PiT-2 deficient VSMCs 36
3.2.3 OC differentiation not observed in PiT-2 deficient VSMCs 37
3.2.4 Knockdown of PiT-2 reduced production of OPN and OPG 38
3.2.5 Knockdown of PiT-2 increased susceptibility of VSMC to cell death 40
3.3 Characterization of PiT-2 ΔSM mouse model 41
3.3.1 SM22α-Cre recombinase mediated genomic DNA rearrangement of conditional PiT-2 alleles 41
3.3.2 SM22α expressed in VSMCs in the aorta, basal ganglia and thalami 43
3.3.3 PiT-2 ΔSM mice did not develop BGC 44
3.3.4 Knockout of PiT-2 in VSMCs did not alter CSF Pi levels 44

Chapter 4. Conclusion and Future Work 46

4.1 Summary and Conclusion 46
4.2 Future work 48
4.2.1 Pi uptake-independent mechanisms of PiT-2 48
4.2.2 Regulation of PiT-2 49
4.2.3 Generation of ciliated epithelial cell-specific PiT-2 knockout model 50

List of References 51

List of Figures

Figure 1: Mechanisms of VC. 9
Figure 2: Generation of PiT-2 conditional (fl/fl) and recombined (ΔSM) alleles. 25
Figure 3: PiT-2 haploinsufficient mice develop BGC. 30
Figure 4: Association of BGC lesions with cerebral arterioles. 31
Figure 5: Localization of PiT-2 to arteriolar VSMCs. 31
Figure 6: PiT-2 expression in CP Ep and Ep and PiT-2 regulation of CSF Pi levels. 33
Figure 7: Effect of PiT-2 specific siRNA on WT VSMCs. 34
Figure 8: Sodium-dependent Pi uptake levels following PiT-2 KD. 35
Figure 9: High-Pi induced calcification of PiT-2 VSMCs. 35
Figure 10: Analysis of secreted PPi levels following PiT-2 KD. 36
Figure 11: Analysis of OC differentiation following PiT-2 KD. 37
Figure 12: Expression and secretion of calcification inhibitors OPN and OPG following PiT-2 KD. 39
Figure 13: Levels of cell death following PiT-2 KD. 40
Figure 14: Genomic DNA arrangement of PiT-2 conditional allele. 42
Figure 15: SM22α IF staining in aorta and brain of PiT-2 fl/fl and ΔSM mice. 43
Figure 16: Alizarin Red S staining in brain coronal sections. 44
Figure 17: Analysis of CSF Pi levels. 45
Figure 18: Summary of proposed two-hit mechanism underlying BGC. 48

List of Tables

Table 1: Primer and probe sequences or assay information for qPCR. 23
Table 2: DNA extraction from tissues: incubation times and elution volumes 26
Table 3: Expression levels of calcification inhibitors identified by RNA-Seq. 39

List of Abbreviations

AIC	Arterial intimal calcification
ALP	Alkaline phosphatase
AMC	Arterial medial calcification
ANOVA	Analysis of variance
APS	Adenosine 5'-phosphosulfate
ATP	Adenosine triphosphate
BCA	Bicinchoninic acid
BGC	Basal Ganglia Calcification
BMP	Bone morphogenic protein
Bp	Base pair
BSA	Bovine serum albumin
BSS	Basal Salt Solution
$CaCl_2$	Calcium chloride
cDNA	Complementary DNA
CKD	Chronic kidney disease
CP	Choroid plexus
CSF	Cerebrospinal fluid
CT	Computerized tomography
DAPI	4',6-Diamidino-2-Phenylindole, Dihydrochloride
DMEM	Dulbecco's Modified Eagle Medium
DNA	Deoxyribonucleic acid
dNTP	Deoxynucleotide
EBSS	Earle's Buffered Salt Solution
ECM	Extracellular matrix
ELISA	Enzyme-linked sandwich assay
FBS	Fetal Bovine Serum
FGF	Fibroblast growth factor
FLP	Flippase
FPKM	Fragments Per Kilobase of transcript per Million
FRT	FLP recombinase target
GFAP	Glial fibrillary acidic protein
HCl	Hydrochloric acid
HEPES	4-(2-hydroxyethyl)-1-piperazineethanesulfonic acid
IBGC	Idiopathic Basal Ganglia Calcification
IF	Immunofluorescence
IgG	Immunoglobulin G
KCl	Potassium chloride
KD	Knockdown
kDa	Kilodalton
KO	Knockout
MGP	Matrix gla protein
MMP	Matrix metalloproteinase

mRNA	Messenger RNA
MV	Matrix vesicles
NaCl	Sodium chloride
NaOH	Sodium hydroxide
NEAA	Non-Essential Amino Acids
OC	Osteochondrogenic
OCN	Osteocalcin
OPG	Osteoprotegerin
OPN	Osteopontin
PBS	Phosphate Buffered Saline
PCR	Polymerase chain reaction
Pi	Inorganic phosphate
PPi	Pyrophosphate
PTH	Parathyroid hormone
qPCR	Quantitative PCR/real-time PCR
RANK	Receptor activator of NF-κB
RANKL	Receptor activator of NF-κB ligand
RNA	Ribonucleic acid
RNase I	Ribonuclease I
RPM	Revolutions per minute
RT	Room temperature (22-24°C)
Runx2	Runt-related transcription factor 2
Scr	Scramble siRNA
siRNA	Small interfering RNA
SM-MHC	Smooth muscle-myosin heavy chain
SM22α	Smooth muscle cell protein 22-alpha
SMA	Smooth muscle α-actin
TNF	Tumor necrosis factor
VC	Vascular calcification
VSMC	Vascular smooth muscle cell
vWF	von Willebrand factor
WT	Wild type
Z-VAD-FMK	Carbobenzoxy-valyl-alanyl-aspartyl-[O-methyl]-fluoromethylketone

Acknowledgements

This degree would not have been possible without significant guidance, encouragement and support from many individuals including my family and friends who have accompanied me on this journey, and the mentors I have had the privilege of working with in the past 4 years.

First and foremost, I would like to thank my advisor Dr. Ceci Giachelli for the opportunity to work on this exciting project, and for her guidance over the past few years. I am grateful for her commitment to my learning and her dedication to making me a better scientist. I would also like to thank Dr. Marta Scatena, as my committee member and also as the graduate program advisor, for her input and guidance in the completion of this work and this degree. Many thanks are also owed to Dr. Mei Speer who has provided an immeasurable amount of help in the planning, execution, and troubleshooting of many of my experiments. I am also especially grateful to Liz Soberg who has shared her experience and expertise, especially in animal work, with me. Her contributions have been instrumental in the completion of this work. Another group of individuals crucial to the completion of this degree was the other talented members of the Giachelli lab, both past and present. I would like to thank them for providing a wealth of scientific knowledge and technical expertise, for ALL the help they have provided, and for the friendships and time spent together outside the lab.

I would also like to acknowledge my family and friends, who have been the core of my support network, not only during my time here in Seattle but also throughout my life. Despite having never met before becoming roommates, Jasmin became my first and closest friend in Seattle. I am so glad that we started (and survived) this graduate school journey together and that we can discuss virtually everything from $6 pea coats to animal studies. My best friends from

middle school, Eehui and Kai Yun have been more than encouraging in lending an ear especially when science did not go my way. I am truly grateful for the past 11 years of friendship, highly motivating pep talks, and prayers despite being more than 8000 miles away. My boyfriend, Yen has provided me with an immense amount of support and love from afar. He has been my fiercest advocate and has never failed to motivate me with his optimism on my low days. I am thankful for the time he has spent and the 50,000+ miles he has flown just to visit me in the past 4 years. Last but not least, this journey would not have been possible without the contributions, wholehearted support and unconditional love from my grandparents and my parents. I am forever indebted to them for constantly encouraging the importance of hard work and the pursuit of knowledge. Without them, I would not be where I am today.

Dedication

To my grandparents and my parents,

thank you for everything!

Introduction

Idiopathic basal ganglia calcification (IBGC) is an autosomal dominant inherited neurodegenerative disorder that results in bisymmetrical calcification in the basal ganglia and other brain regions, such as the thalamus, dentate nucleus and cerebral cortex[1]. The calcification is associated with the medial layer of small cerebral arteries, arterioles and capillaries, but not veins[2–4]. Patients with IBGC display a wide variety of symptoms that worsen with age, including vascular dementia, hallucinations, motor control disorders, migraines and strokes[5–7]. However, they develop minimal calcification in the peripheral vasculature and have normal serum levels of calcium, inorganic phosphate (Pi), alkaline phosphatase (ALP), vitamin D and parathyroid hormone (PTH)[8,9]. Currently, there are no therapeutic drugs available for IBGC or vascular calcification (VC) in general, and treatments for IBGC only focus on symptomatic relief[10].

Human genome sequencing studies have identified the association of IBGC with mutations in SLC20A2, PDGFB, PDGFRB and most recently, in XPR1[7,9,11–14]. Mutations in SLC20A2, a gene that encodes the Type III sodium-dependent Pi transporter, PiT-2, are found in approximately 50% of the IBGC cases[8,11,15,16]. We and others have shown that the removal of PiT-2 in mice resulted in bilateral brain calcification, accurately recapitulating the human disease and demonstrating that reduced PiT-2 expression alone can cause brain calcification[16,17]. However, the etiology underlying IBGC and the mechanisms by which PiT-2 mediates its protective effect are currently unknown.

This study focused on PiT-2 in vascular smooth muscle cells (VSMCs), the major cellular component of the medial layer that is associated with the calcification observed in IBGC patients. Previous studies have shown that VSMCs play a major role in the development of VC

seen in atherosclerosis, diabetes, and chronic kidney disease (CKD)[18–21]. However, whether VSMCs play a role in the development of VC in IBGC has not yet been evaluated. To this end, the goals of the present study were to develop a PiT-2 deficient model in VSMCs and to make use of this model to determine the protective mechanism of PiT-2 that underlies IBGC. In addition, this study aimed to generate a VSMC-specific PiT-2 knockout mouse model, and to determine if these mice developed BGC.

In addition to IBGC, basal ganglia calcification (BGC) itself is common and is indistinguishable from IBGC radiologically. BGC occurs in up to 1.5% of individuals who undergo a CT scan[22], and is especially common in those with hypoparathyroidism[23]. Understanding how to target and treat IBGC can benefit not only patients with IBGC but also those with hypoparathyroidism or other diseases that also cause secondary BGC. Ultimately, this understanding may be used to identify novel therapies that could prevent the development and progression of BGC and improve overall patient health.

This thesis is presented in four chapters. Chapter 1 details the background and significance of IBGC, PiT-2, VSMCs and the current understanding of the mechanisms underlying VC. Chapter 2 describes the materials and methods used in this study. Chapter 3 discusses the hypotheses and results of the study, and Chapter 4 presents a summary of the work, conclusions, and possible directions for future work.

Chapter 1. Background and Significance

1.1 IBGC

IBGC, originally known as Fahr's disease, is a rare neurodegenerative disease that affects approximately one in a million people[10]. The age of onset is typically in the fourth or fifth decade, although this disorder can present itself in childhood or later in life. It can occur without a genetic or familial component, or can be inherited in an autosomal dominant manner[24], where the age of disease onset decreases progressively with each transmission within the family[25]. The disease is characterized by abnormal bilateral calcium phosphate salt deposits in the basal ganglia and also in other brain regions, such as the thalamus, dentate nucleus and cerebral cortex[1]. Specifically, the calcification is associated with the medial layer of small cerebral arteries, arterioles and capillaries, but not veins[2–4,26]. In contrast with ectopic VC in patients with atherosclerosis, diabetes, and CKD that are often associated with secondary calcium, Pi, hormonal and/or metabolic imbalances, IBGC patients have minimal calcification in peripheral vasculature and have normal blood calcium, Pi, ALP, vitamin D and PTH levels[8,9,27]. These patients display a wide spectrum of symptoms that worsen with age, including vascular dementia, hallucinations, motor control disorders, migraines and strokes[1,7,12,15,28]. Of note, ischemic stroke has been reported in a patient with IBGC[29], and brain calcification has been observed in stroke patients in general[30]. In addition, intracranial artery calcification is a newly identified risk factor for ischemic stroke, correlated with higher incidences of stroke[31,32]. However, the severity of IBGC can be very heterogeneous among individuals as well, as there have also been cases where brain calcification is detected as an incidental finding in asymptomatic individuals[33].

Calcification of the basal ganglia can be a nonspecific finding in many medical conditions, including infectious, metabolic, and genetic diseases. In addition, BGC is found in 0.7% to 1.5% of brain computerized tomography (CT) scans, and even in up to 70% of individuals with hypoparathyroidism[22,23,34–36]. However, these incidental findings of calcification are usually benign and have no clear etiology[36]. Due to the presence of symptoms very similar to other neurological diseases and the inability to radiologically differentiate IBGC from BGC resulting from other causes, diagnosing IBGC has been challenging. In addition to the visualization of bilateral calcification of the basal ganglia on CT scans, patients must also present progressive neurologic dysfunction, the absence of any infectious, metabolic, toxic or traumatic causes, the absence of biochemical and hormonal abnormalities, and a family history consistent with autosomal dominant inheritance[33,37] to be diagnosed.

Currently, there are no specific therapeutic drugs available for BGC and current treatments only aim to alleviate the symptoms[10]. There have only been a few reports showing the effectiveness of anti-psychotic drugs and antidepressants in treating IBGC patients with schizophrenia-like psychosis and obsessive-compulsive behaviors, although the ability of these drugs to stabilize or to reduce the calcified lesions has not been evaluated[28,38,39]. Recently, a study reported possible symptomatic improvements in several patients treated weekly with alendronate, a widely prescribed bisphosphonate, although the results were inconsistent due to the low sample size evaluated. There was also no clear change in brain imaging patterns over the treatment period in these patients[40]. Therefore, there is an urgent need to address treatment options that target the calcification itself.

Recent genome sequencing studies have identified the association of IBGC with mutations in SLC20A2, PDGFB, PDGFRB and most recently, in XPR1[7,9,11–14]. Approximately

50% of IBGC patients have mutations in SLC20A2, a gene that encodes a type III sodium-dependent Pi transporter PiT-2, which will be discussed in Section 1.2[8,11,15,16]. In addition, no genotype-phenotype correlations have been observed in individuals with mutations in PiT-2[8]. However, IBGC cases with mutations in these known genes do not account for all of the IBGC cases, suggesting there could be other genes whose involvement has yet to be discovered and identified.

The focus of this research study was to study the role of PiT-2 in BGC, as the number of cases associated with mutations in PiT-2 make up the majority of all IBGC cases, and IBGC patients with mutations in PiT-2 also develop more severe calcification compared to patients with mutations in the other genes[7,33].

1.2 Sodium-dependent Pi transporters

Pi transport across the cell membrane is essential for normal cellular function, signaling and metabolic pathways[41]. Therefore, it is critical that serum Pi levels in the body are tightly regulated. In mammals, three types of sodium-dependent Pi transporters have been identified: SLC17 (Type I), SLC34 (Type II), and SLC20 (Type III). Although SLC17 transporters are expressed in the kidney, liver and brain (at very low levels), their role in Pi homeostasis is still largely unknown[42]. SLC34 transporters are expressed on specific organs important for Pi homeostasis, including the kidney and the intestine, and they play a major role in tightly regulating Pi absorption and reabsorption in order to maintain normal serum Pi levels between 0.8 and 1.5 mM[43]. Lastly and most relevant to this study, the two SLC20 transporters, SLC20A1 and SLC20A2, are ubiquitously expressed in all tissues and were generally considered "housekeeping" transport proteins. However, recent studies have revealed their tissue-specific activities, regulatory pathways, and even signaling capabilities[41,44].

SLC20A1 and SLC20A2, encoding PiT-1 and PiT-2 respectively, were originally identified as retroviral receptors - gibbon ape leukemia virus receptor (Glvr-1) and rat amphotropic leukemia virus receptor (Ram-1)[45,46]. Their role as high affinity, low capacity sodium-dependent Pi transporters was only identified shortly after[47,48]. The transport of Pi in PiT-1 and PiT-2 involves the initial binding of a Na^+ ion, followed by a random interaction of monovalent Pi and a second Na^+ ion[49]. Reorientation of the transporter then leads to substrate release in the cytosol. Topology models of these two transporters show twelve predicted transmembrane domains and an intracellular domain, with extracellular N- and C-terminal tails[50–52]. Despite their similarities in their structures and transport kinetics, PiT-1 and PiT-2 differ in virus binding locations; for PiT-1, this occurs at the fourth extracellular loop while for PiT-2, it occurs at the first extracellular loop[53,54].

The physiological role of PiT-1 has been more widely researched. An *Slc20a1* knockout mouse developed anemia and abnormal yolk sac vasculature development, reduced proliferation and induced massive apoptosis of liver cells, and resulted in embryonic lethality, demonstrating the importance and non-redundant role of PiT-1 in embryonic development[55,56]. PiT-1 has also been shown to play a role in high Pi-induced matrix calcification[57], terminal erythroid differentiation and early B-cell development[58], and parathyroid function[59]. Recently, novel Pi uptake-independent functions of PiT-1 have also been discovered, suggesting that PiT-1 could also have signaling functions[44,60,61].

On the other hand, aside from its genetic association with IBGC, less is known about the functional role of PiT-2[8,11,15,16]. The type and location of the PiT-2 mutations associated with IBGC vary. Currently, 50 mutations have been identified, affecting all exons except exon 6. Mutations include missense (46%), frameshift (20%), splice-site (14%), nonsense (14%), indel

(4%) and copy number variations (2%)[27]. Some mutations lead to truncated PiT-2 mRNA which is most likely degraded, while others translate into PiT-2 mutant proteins that are shown or predicted to be unable to transport Pi[8,11,15,27,62]. However, no correlation has been found between the type of mutation and the severity of the calcification, or clinical and radiological presentations[8,33].

1.3 VC

VC is the abnormal deposition of calcium phosphate salts on arterial walls and heart valves. It is often seen in normal aging, and in patients with CKD, diabetes, or atherosclerosis. There are two main types of calcification in blood vessels—intimal calcification and medial calcification, affecting the intimal and medial layers of vessels respectively. Despite being described as distinct forms of calcification based on the vessel layer it affects, it is hard to differentiate the location of intimal calcification from medial calcification in a vessel, even with the most advanced imaging modalities available[63].

Arterial intimal calcification (AIC) is characterized by lipid deposition, inflammation, and plaque formation in the subintima, ultimately resulting in obstruction of the arterial lumen. AIC is strongly associated with atherosclerosis and the development of plaques containing a fibrous cap enclosing a lipid-rich necrotic core. Plaque development is complex and dynamic, involving interactions between factors and multiple cell types including VSMCs, endothelial cells, leukocytes and macrophages[64]. The exact reason for the thinning and the eventual rupture of the plaque is unknown, but calcification can increase the susceptibility of plaques to rupture[65]. Plaque rupture leads to potential thrombosis and subsequent myocardial infarction, stroke and death[66]. Of note, death due to atherosclerosis accounts for approximately 50% of all cardiac-related deaths[67].

On the other hand, arterial medial calcification (AMC) is characterized by arterial stiffening and calcium phosphate deposition within the elastin layers of the medial layer and without any form of lumen obstruction. This is often seen in aging patients, and is especially severe in patients with diabetes or CKD. AMC results in loss of vessel compliance, increased pulse wave velocity and pulse pressure. The increase in vascular stiffness also leads to decreased coronary perfusion, left ventricular hypertrophy, hypertension, and eventually, heart failure[68–70]. In addition, the presence of AMC is also a strong predictor of cardiovascular events and mortality in patients with CKD[21,69]. The type of calcification IBGC patients develop is characteristic of medial calcification, and therefore the focus of this study was to explore mechanisms specific to AMC.

VC was once thought to be a consequence of aging and to result from a passive deposition of calcium phosphate salts on the extracellular matrix (ECM), but recently, VC has been recognized as an active and complicated cell-mediated process[71]. However, the specific etiology still remains unclear. Several proposed mechanisms include: failed anticalcific processes, osteochondrogenic (OC) differentiation, cell death, extracellular matrix (ECM) degradation and dysregulated mineral metabolism (Fig. 1). The following sub-sections will first describe the VSMC, an important cell type that plays a major role in VC, and discuss the individual relevant mechanisms of VC in detail.

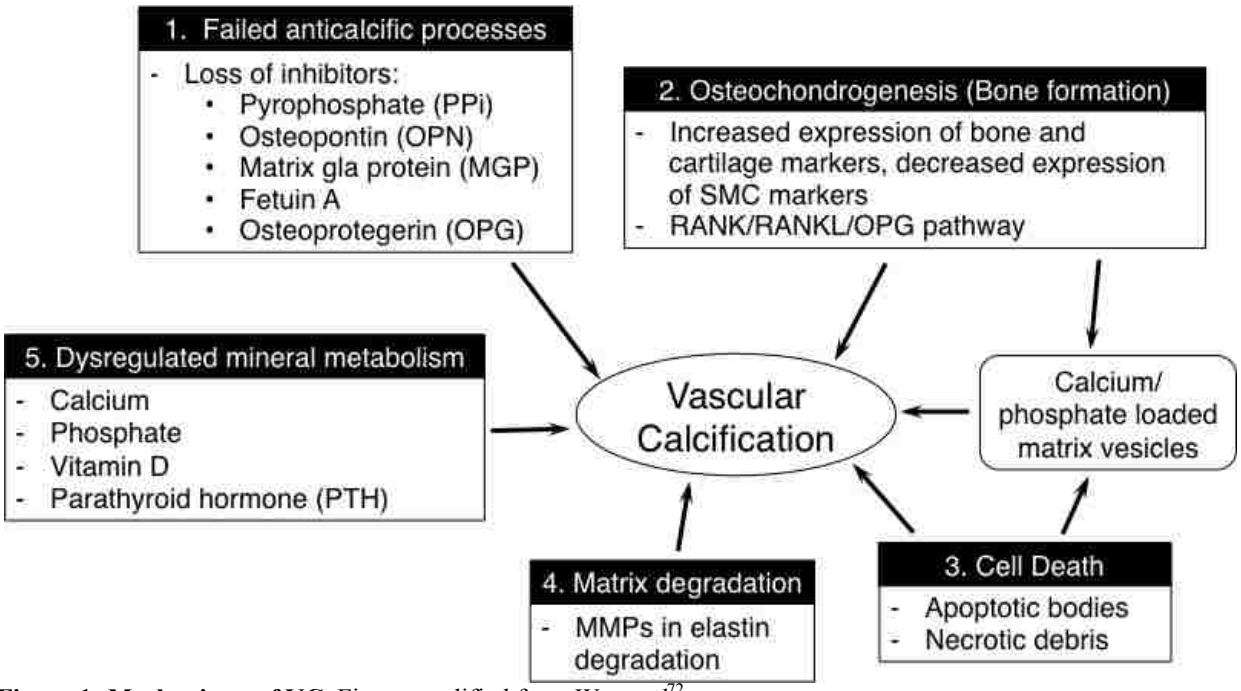

Figure 1: Mechanisms of VC. Figure modified from Wu *et al*[72].

1.3.1 VSMCs

VSMCs are the contractile cells found in the medial layer of vessels that normally maintain the vascular tone of the vessel. By contraction and relaxation, the luminal diameter of the vessel can be regulated, allowing blood vessels to maintain appropriate blood pressure[73]. VSMCs also play an important role in vessel remodeling in physiological conditions such as exercise and pregnancy, but more importantly, after vascular injury, indicating their phenotypic plasticity.

The ability of VSMCs to exhibit phenotypic diversity has long been recognized. The normal phenotype in which most of the VSMCs exist in the medial layer is often known as the differentiated contractile phenotype. This phenotype is characterized by high expression of VSMC-related genes including α-smooth muscle (SM)-actin (SMA), SM22α, and SM-myosin heavy chain (SM-MHC)[74] that are involved in maintaining myofilament structure and function. During long-term culture *in vitro*, injury, or progression of VC, VSMCs spontaneously undergo

de-differentiation into a synthetic phenotype that expresses lower levels of VSMC-related genes and contains fewer myofilaments[73]. VSMC phenotypic switch is often stimulated by injury, and the switch is essential for the process of vascular repair, during which VSMCs migrate, proliferate and elaborate an appropriate ECM. In atherosclerosis, VSMCs migrate from the medial layer to the intimal layer to form a VSMC-rich fibrous cap that shields the lipid-rich core from blood flow.

Contractile and synthetic phenotypes are the most extreme ends of the phenotypic diversity VSMCs can possess; in fact, recent studies have shown that the synthetic phenotype might be more heterogeneous and complicated than previously described. Multiple *in vitro* and *in vivo* studies have also demonstrated that phenotypic change is associated with the ability of VSMCs to acquire characteristics of other mesenchymal lineages such as osteoblastic and chondrocytic, both of which are observed in VC[18,75–78,71].

1.3.2 Failed anticalcific processes

Genetic studies in humans and mice have shown that the blood vessel normally expresses mineralization inhibitors such as pyrophosphate (PPi), matrix gla protein (MGP), osteoprotegerin (OPG). The lack of these molecules or proteins leads to spontaneous calcification of arteries and cartilage. Fetuin A is also a potent inhibitor that is also present in circulation, and decreased levels of fetuin A have been correlated with accelerated calcification and cardiovascular mortality in CKD patients, suggesting its role in normally protecting vessels from calcification[79–83]. Osteopontin (OPN), on the other hand, is not normally expressed in vessels, but is highly upregulated during the calcification process, especially upon vessel injury[84]. In addition, phosphorylated OPN has also been shown to prevent mineralization of VSMCs *in vitro*[85]. These studies suggest that PPi, MGP, OPG, fetuin A and OPN may be naturally occurring inhibitors of

calcification, and are either constitutively expressed or injury-induced in arteries to prevent mineralization[86].

1.3.3 OC differentiation

Recent data have presented the similarities between vascular calcification and bone formation. Of note, bone matrix and morphogenic proteins involved in regulating normal bone development and osteogenesis have been identified in calcified tissues. These proteins, expressed by VSMCs include bone morphogenic protein (BMP)-2, BMP-4, BMP-6[87–89], osteonectin[90] and OPN[74,80,84,90–93]. In addition, VSMCs have the ability to mineralize *in vitro*, either with the addition of Pi or beta-glycerophosphate, and to adopt a phenotype and expressing several genes important for bone mineralization similar to that of osteoblast-like cells[94–96]. Specifically, elevated Pi levels induced VSMCs to undergo an OC phenotype change characterized by the loss of SMC markers, such as SM22α and SMA, and the gain of OC markers, such as OPN, osteocalcin (OCN), ALP and runt-related transcription factor 2 (Runx2)[18].

In addition, the OPG/receptor activator for NF-κB (RANK)/RANK ligand (RANKL) triad, molecules of the tumor necrosis factor (TNF)-related family, have also been suggested to play a role in the development of VC, even though their exact roles in VC have not been fully elucidated. OPG is a soluble decoy receptor for RANK, while RANK binds to its ligand RANKL to regulate differentiation, maturation, and activation of osteoclasts, and therefore regulating the critical balance of bone resorption by osteoclasts and bone formation by osteoblasts. RANKL has been shown to increase VSMC calcification *in vitro* via alternative NF-κB pathways such as the induction of interleukin-6 or the activation of the RANK-BMP4 pathway, and the RANKL-dependent calcification was abrogated with the introduction of OPG[97,98]. These results suggest

that OPG can neutralize the pro-calcifying effects of RANKL, further strengthening the idea that the process of VC heavily mirrors that of bone formation.

1.3.4 Cell death

Cell death is another potential mechanism that may play a role in VC. In a study by Ewence *et al*., calcium phosphate crystals induced rapid rises in intracellular calcium concentration and subsequently apoptotic cell death in human aortic VSMCs *in vitro*, and the potency of the crystals depends on their size and composition[99]. Matrix vesicles (MVs) can also serve as nucleating structures for hydroxyapatite crystal formation, both in normal bone formation and also in VC[100,101]. In addition, the process of MV production and regulation is thought to be associated with apoptotic cell death. Of note, apoptotic bodies derived from VSMCs were shown to initiate mineralization in an *in vitro* human VSMC model, and the calcification was ameliorated after treatment with Z-VAD-FMK, a widely used inhibitor of apoptosis[102]. Necrosis, on the other hand, is usually a result of injury or inflammation, and is frequently seen in atherosclerosis. The development of the necrotic core in an atherosclerotic plaque may eventually lead to calcification of the lesion and the surrounding tissue[103].

1.3.5 ECM remodeling

ECM remodeling, specifically elastin layer fragmentation, has also been shown to lead to calcification. Elastin plays a major role in maintaining vessel compliance, and the calcification of the elastin layers leads to increased stiffness and the loss of vessel compliance characteristic of AMC, and overall mortality in patients with CKD[68,104]. Elastin degradation also increases the affinity of the ECM to calcium, and this degradation process is mediated by several proteases such as matrix metalloproteases (MMPs) and cathepsin S[68,105–107]. Not surprisingly, rats subdermally implanted with purified elastin fragments develop severe calcification, and the

delivery of MMP inhibitors significantly reduced elastin calcification[106]. Although elastin fragmentation itself is not sufficient to cause AMC, it is suggested that sites of degradation may serve as calcification-prone sites that are subject to subsequent calcium phosphate salt deposition following another stimulus such as altered mineral metabolism that will be detailed in the next section[105].

1.3.6 Dysregulated mineral metabolism

Dysregulated mineral metabolism plays a role in the development and worsening of VC. These factors include serum levels of calcium, Pi, vitamin D and PTH.

Hyperphosphatemia is a major inducer of VC, playing a role in genetic diseases and especially in patients with renal failure. Patients with mutations in the genes for fibroblast growth factor (FGF)-23, a major phosphaturic hormone; klotho, a cofactor for FGF; and GALNT3, a UDP N-acetyl-α-D-galactosamine, develop familiar tumoral calcinosis and hyperphosphatemia[108–110]. Elevated serum Pi levels is positively correlated with morbidity and mortality, and the risk of death dramatically increases when serum levels of Pi exceed 6.5 mg/dL (2.1 mM)[111]. In addition, animal models of CKD rely on high Pi diet feeding to induce AMC and fully recapitulate CKD in mice with compromised kidney function[112,113]. Hypercalcemia is also often observed in patients with familial tumoral calcinosis, as well as CKD[21,108]. *In vitro* studies have also shown that exposing human VSMCs to elevated extracellular calcium levels can increase mineralization. This mineralization is further exacerbated when extracellular Pi levels were increased to levels of hyperphosphatemia, suggesting that the effects of calcium and Pi are often synergistic[114]. Indeed, elevated serum levels of the calcium phosphate product (Ca x P) predisposes patients to VC, and are associated with increased mortality and morbidity in patients with CKD[115,116].

The role of vitamin D is well established in skeletal biology, but its role in VC is complex. Both the excess and deficiency of vitamin D have been associated with VC, indicating a biphasic effect. Severe vitamin D deficiency is observed in CKD patients with VC due to their reduced ability to convert the inactive forms of vitamin D to its physiologically active form, 1,25-dihydroxyvitamin D. As a result, administration of active forms of vitamin D have been attempted as a form of therapy but the association between vitamin D and improved survival have not been shown[117,118]. In fact, higher incidences of calcification have been observed in patients undergoing vitamin D therapy[119]. Consistent with human observations, injections of high doses of vitamin D result in severe calcification in rodents but the vitamin D-induced VC has also been shown to be reversible[120]. However, on the other hand, calcification has also been observed with low non-hypercalcemic doses of vitamin D[121], further strengthening the bimodal effect of vitamin D on calcification and highlighting the importance of specific dosage levels in using vitamin D as a form of therapy for VC. One possible reason for inconsistency is the ability of 1,25-dihydroxyvitamin D to act as a hormone and to exhibit endocrine effects on the kidney, intestine, parathyroid, and bone, which in turn affects the levels of calcium, Pi and PTH as well.

Hyperparathyroidism has been associated with increased levels of calcification and mortality rates in patients with CKD[122]. Consistent with human findings, rats injected with PTH developed severe AMC. In addition, vitamin D deficiency is also associated with secondary hyperparathyroidism, which in turn exacerbates the extent of calcification. There is also substantial evidence suggesting that hypoparathyroidism leads to VC, despite inconsistent results in CKD patients [123,124], and approximately 70% of patients with hypoparathyroidism develop secondary BGC[22].

1.4 Tissue-specific gene deletion

The most widely used method to generate gene knockout models is using the Cre/loxP recombination method, which induces site-specific recombination. This method makes use of two components: Cre recombinase and loxP recognition sites. Cre recombinase is a 38 kDa protein, part of the integrase family of recombinases that catalyzes the site-specific recombination without any need for cofactors or complementary proteins. LoxP sites are 34 base pair (bp) long recognition sequences that include two 13-bp long palindromic repeats separated by an 8-bp long asymmetric core spacer that determines the directionality of the sequence[125]. These loxP sequences are deliberately inserted at specific locations in a DNA sequence, allowing for targeted and effective genomic manipulation. Usually the loxP sequences flank a sequence in an essential exon that ideally results in a non-functional null allele. However, there is always the risk that the resulting allele will result in a product that has residual function[126].

During recombination, a Cre protein binds to each of the 13-bp repeat sequences on a single loxP site, forming a Cre dimer. When two loxP sites align in parallel orientation, it allows the four Cre proteins to form a tetramer and a double-strand break occurs in the 8-bp spacer region. The sequence between the inserted loxP sites is excised as a circular piece of DNA that is subsequently degraded, and the original DNA sequence recombines, leaving a single loxP site at the location of excision[127]. Besides Cre-dependent gene deletion, this versatile Cre/loxP recombination method can also be used in other genome editing applications, such as Cre-dependent gene expression and selection marker removal[126].

By placing the Cre recombinase downstream of promoters that are active only in a certain cell or tissue type, or during a specific stage of embryonic development, a tissue-specific knockout mouse model can be generated. This allows for a targeted gene to be specifically

removed from a specific cell type or tissue(s) while in other cell types or tissues, the gene remains functionally expressed. A tissue-specific knockout model provides many advantages over traditional gene knockout models. In traditional gene knockout models, knockout of certain genes, especially those critical to development may often lead to embryonic lethality, preventing the study of those genes in adults. On the other hand, tissue-specific knockout models provide the ability to study the effect of one gene in isolation, in a specific cell type or tissue at a specific time.

Chapter 2. Materials and Methods

2.1 Materials

2.1.1 Tissue culture reagents

Antibiotic-antimycotic, HEPES, high glucose, L-glutamine and Phenol Red supplemented Dulbecco's Modified Eagle Medium (DMEM), L-glutamine, Lipofectamine RNAiMAX, LIVE/DEAD Viability/Cytotoxicity Kit, MEM Non-Essential Amino Acids (NEAA) solution, Opti-MEM, Silencer Select Negative Control No. 1 siRNA, Silencer Select Pre-Designed siRNA for PiT-2 (Slc20a2), trypsin, and Versene solution were obtained from ThermoFisher Scientific (Waltham, MA). Collagenase type II, elastase and soybean trypsin inhibitor were obtained from Worthington Biochemical Corporation (Lakewood, NJ). Phosphorus-33 (^{33}P) was purchased from PerkinElmer (Waltham, MA), fetal bovine serum (FBS) was purchased from Atlanta Biologicals (Flowery Branch, GA), and staurosporine was purchased from Abcam (Cambridge, MA).

2.1.2 Other reagents

Adenosine triphosphate (ATP) sulfurylase, boric acid, DAPI dilactate, Micro BCA Protein Assay Kit, sodium borate decahydrate, sodium chloride, sodium citrate dehydrate, sodium pyrophosphate decahydrate, TaqMan Gene Expression Assays, TaqMan Ribosomal RNA Control Reagents, Tris Base, Permount, and ProLong Gold Antifade Mountant were obtained from ThermoFisher Scientific (Waltham, MA). Adenosine 5'-phosphosulfate (APS) sodium salt, Alizarin Red S, ATP assay mix, ATP disodium salt hydrate, ethidium bromide, fraction V bovine serum albumin (BSA), phosphate buffered saline (PBS) powder, and goat immunoglobulin G (IgG) were purchased from Sigma-Aldrich (St. Louis, MO). DNeasy Blood

& Tissue Kit, Omniscript Reverse Transcription Kit, RNeasy Mini Kit, and RNeasy Protect Animal Blood Kit were purchased from Qiagen (Hilden, Germany). Mouse Osteopontin DuoSet ELISA and mouse Osteoprotegerin/TNFRSF11B Quantikine ELISA Kit were purchased from R&D Systems (Minneapolis, MN). Cy3 AffiniPure Donkey Anti-Goat IgG (H+L) was purchased from Jackson ImmunoResearch Labs (West Grove, PA), QuantiChrom Phosphate Assay Kit was purchased from BioAssay Systems (Hayward, CA), goat polyclonal SM22α antibody was purchased from Abcam (Cambridge, MA) and Calcium Reagent Set was purchased from Teco Diagnostics (Anaheim, CA).

2.1.3 Laboratory equipment

A P-87 flaming micropipette puller from Sutter Instrument Company (Novato, CA) was used to pull glass capillary tubes for cerebrospinal fluid (CSF) collection. ABI Prism 7000 Sequence Detection System from Applied Biosystems (Foster City, CA) was used for quantitative polymerase chain reaction (qPCR) amplification and detection. Nikon (Melville, NY) TE200 and E800 microscopes were used for image capture. A TD-20/20 luminometer from Promega (Madison, WI) was used for measuring bioluminescence for the PPi assay. An LS 6500 liquid scintillation counter from Beckman Coulter (Brea, CA) was used to measure ^{33}P radioactivity for the Pi assay.

2.1.4 Software

SDS 1.1 from Applied Biosystems (Foster City, CA) was used for the analysis of qPCR results. ImageJ from the National Institutes of Health (Bethesda, MD) was used for image processing and quantification. Nikon NIS-Elements (Melville, NY) was used for image capture.

2.2 Methods

2.2.1 VSMC isolation and culture

VSMCs were isolated from 4 to 5-week-old WT mice of C57BL/6J origin. The arch, thoracic aorta and the upper part of the abdominal aorta were dissected, cleaned of the connective and were first incubated in a digestion solution containing 1 mg/mL collagenase type II, 0.23 mg/mL elastase, 0.375 mg/mL soybean trypsin inhibitor, and 2 mg/mL BSA in DMEM with 1X antibiotic-antimycotic for 4 min at 37°C to separate the media from the adventitia. Vessels were cut longitudinally and endothelial cells were removed with a wetted sterilized cotton swab. The media was peeled off from the adventitia, cut into 3-5 mm pieces, and digested in a second digestion solution containing 0.64 mg/mL collagenase type II and 20% FBS in DMEM with 1X antibiotic-antimycotic for 20 min in a water bath at 37°C. Samples were spun down at 500 RPM for 1 min, rinsed once with DMEM with 1X antibiotic-antimycotic, and incubated in a final digestion solution containing 0.64 mg/mL collagenase type II, 0.44 mg/mL elastase, and 20% FBS in DMEM with 1X antibiotic-antimycotic for 30-35 min in a water bath at 37°C with occasional gentle agitation to release the VSMCs from the media. To stop the digestion, an equal volume of ice-cold DMEM with 1X antibiotic-antimycotic was added. The cell suspension was centrifuged at 1000 RPM for 5 min, the pellet was resuspended in DMEM with 20% FBS, 1% NEAA, 1% glutamine, 1X antibiotic-antimycotic, and seeded into a pre-equilibrated T-25 flask. The flask was then incubated for 3 days to allow the cells to spread and attach to the flask. VSMCs were split 1:2 when confluent. VSMCs of at least 95% purity, characterized by the presence of SM22α, SMA and von Willebrand factor (vWF), were used for cell culture studies. Subcultured VSMCs were maintained in DMEM with 10% FBS, and cells used for experiments were from passage 7 - 10.

2.2.2 siRNA-mediated knockdown of PiT-2

WT mouse VSMCs were seeded at a density of 2.5 x 10^4 cells/well in a 6-well plate with DMEM with 10% FBS and 1X antibiotic-antimycotic (growth media). After 24 hours, growth media was replaced with DMEM with 10% FBS (transfection media) before 2 nM of siRNA specific to mouse PiT-2 or Silencer Select Negative Control No. 1 (scramble, Scr) siRNA, and 1.5 μL of Lipofectamine RNAiMAX were added to the respective wells. VSMCs without siRNA treatment (no treatment, NT) were also used as a negative control. Transfection media was replaced with growth media after 24 hours. VSMCs were re-dosed with the respective siRNAs after 5 days and transfection media was replaced with growth media after 6 hours. Sense: 5'-GGCGUGCUGUUCAUACUAA-3'; Antisense: 5'- UUAGUAUGAACAGCACGCC-3'.

2.2.3 Pi uptake assay

Pi uptake studies were performed with mouse VSMCs, as previously described[128]. Briefly, WT, Scr or KD VSMCs were incubated in Earle's Buffered Salt Solution (EBSS) containing 0.1, 0.25, 0.5 mM Pi and 5 μCi/mL $H_3{}^{33}PO_4$. Radioactivity was measured by a liquid scintillation counter. Sodium-dependent Pi uptake was determined by subtracting uptake levels measured in EBSS containing choline chloride from uptake levels measured in EBSS containing sodium chloride. Uptake values were normalized to cellular protein content, measured with the Micro BCA Protein Assay.

2.2.4 Calcification assay

VSMC matrix calcification was induced by treatment with DMEM with 3% FBS and 1X antibiotic-antimycotic, supplemented with NaH_2PO_4/Na_2HPO_4 to a final concentration of 2.8 mM Pi (calcification media) for 4 and 6 days to analyze time-dependent levels of calcification. VSMCs treated with DMEM with 3% FBS and 1X antibiotic-antimycotic containing 0.97 mM Pi

were used as controls. Media was replaced every other day. VSMCs were washed 3 times with PBS and decalcified with 0.6N HCl overnight at 4°C. The calcium content was determined colorimetrically by the o-cresolphtalein complexone method (Calcium Reagent Set) at 575 nm. After decalcification, VSMCs were washed 3 times with PBS and solubilized with 0.2N NaOH for protein. The calcium content was normalized to protein content, measured with the Micro BCA Protein Assay.

2.2.5 PPi assay

Secreted PPi was measured using an enzyme-linked bioluminescence assay, as previously described[129]. In the presence of the enzyme ATP sulfurylase, PPi reacts with APS to generate ATP, which is measured by a luciferin/luciferase reaction. Briefly, cultured VSMCs were washed 3 times with sterile PBS, and incubated in 800 µL Basal Salt Solution (BSS) containing 130 mM NaCl, 5 mM KCl, 1.5 $CaCl_2$, 25 mM Na-HEPES (adjusted to pH 7.5), 5 mM D-glucose, and 0.1% BSA for 5 min at 37°C. The BSS was collected and heat-inactivated at 100°C for 5 min and total protein was extracted from the cells by adding 500 µL 0.2N NaOH to each well. 20 µL of 25 µM APS and 4 µL concentrated ATP assay mix were added to 75 µL of BSS sample in a cuvette, and the mixture was immediately measured in a TD-20/20 luminometer to determine the ATP-dependent bioluminescence. 1 µL of 10 units/mL ATP sulfurylase was added to the mixture to drive the conversion of PPi to ATP and the bioluminescence was measured again. The PPi-dependent bioluminescence is determined by subtracting the value of ATP-dependent bioluminescence from the final bioluminescence value, and normalized to time and protein content quantified by the Micro BCA Protein Assay. A PPi standard curve was generated using 1 nM to 100 nM sodium pyrophosphate decahydrate in BSS.

2.2.6 Cell death assay

The amount of cell death in cultured VSMCs was determined by the LIVE/DEAD Viability/Cytotoxicity Kit containing calcein-AM and ethidium homodimer-1 that stain live and dead cells respectively. VSMCs treated with normal Pi media (0.97 mM) or calcification media (2.8 mM Pi) for 2 and 6 days were washed 3 times with PBS, and incubated in a staining solution containing 1 μM calcein-AM and 2.5 μM ethidium homodimer-1 for 30 min in the dark at room temperature (RT). VSMCs treated with 750 nM staurosporine for 20 hours were used as a positive control. The staining solution was removed and replaced with PBS prior to imaging on a Nikon TE200 inverted microscope. For each well, five independent fields of view were imaged. The number of live and dead cells was counted blindly, and the counts in all five fields of view for each well were averaged. The percentage of dead cells per well was quantified by the number of dead cells divided by the total number of cells (number of live and dead cells). Four biological replicates per condition were quantified.

2.2.7 Gene Expression

2.2.7.1 qPCR

cDNA was made with total RNA using the Omniscript Reverse Transcriptase Kit. Each reaction contains 5 μL cDNA and 20 μL 20X TaqMan Gene Expression assay or master mix containing TaqMan Universal PCR 2X Master Mix, dNTPs, forward and reverse primers, and probe. Probes were conjugated with a FAM fluorochrome reporter tag at the 5'-end and with an MGB quencher at the 3'-end. The amplification and quantification of cDNA was done in 96-well optical plates, and carried out at 50°C for 2 min, 95°C for 10 min, 40 cycles of 95°C for 15 seconds, and 60°C for 1 min on an ABI Prism 7000 Sequence Detection System. Results were analyzed using SDS 1.1. Gene mRNA expression was first normalized to the housekeeping gene

18S, and normalized to the respective control using the quantitative $2^{-\Delta\Delta C}{}_T$ method, where $\Delta\Delta C_T = (C_{T,gene} - C_{T,18S})_{treated} - (C_{T,gene} - C_{T,18S})_{control}$.

Table 1: Primer and probe sequences or assay information for qPCR.

Gene	Sequence (5' to 3')
OPG (Tnfrsf11b)	TaqMan Gene Expression assay, Mm00435454_m1
OPN (Spp1)	Forward: TGAGGTCAAAGTCTAGGAGTTTCC Reverse: TTAGACTCACCGCTCTTCATGTG Probe: TTCTGATGAACAGTATCCTG
PiT-2 (Slc20a2) in VSMCs	Forward: GACCGTGGAAACGCTAATGG Reverse: CTCAGGAAGGACGCGATCAA Probe: CATGGTTGGTTCAGCTG
PiT-2 (Slc20a2) in whole blood	TaqMan Gene Expression assay, Mm00660204_mH
Runx2 (Cbfa1)	Forward: CGGGCTACCTGCCATCAC Reverse: GGCCAGAGGCAGAAGTCAGA Probe: CGTATTTCAGATGATGACACTG
SM22α (Tagln)	Forward: GACTGACATGTTCCAGACTGTTGAC Reverse: CAAACTGCCCAAAGCCATTAG Probe: TGAAGGTAAGGATATGGCAGC
18S	18S Ribosomal RNA Control Reagents

2.2.7.2 RNA-Seq

Total RNA sequencing (RNA-Seq) was done on RNA isolated from Scr and KD VSMCs treated with siRNA for 2 and 3 days (n=1) at the High Throughput Genomics Center at the University of Washington. Approximately 5 to 6 x 10^6 cells per condition were prepared for sequencing using an Illumina platform. Total RNA was extracted from the VSMCs and purified using poly-A tail enrichment to generate an mRNA library. The mRNA transcript was hydrolyzed into 200-300 nucleotide fragments for the reverse transcription reaction. The cDNA fragments were sequenced via paired-end sequencing, generating two 76 bp long reads per fragment that were then aligned to a reference mouse genome, mm9. Relative expression levels of the mRNA transcript, proportional to the number of cDNA fragments that originate from it,

were normalized to the total number of mapped reads using the Cufflinks program[130] and quantitatively expressed as Fragments Per Kilobase of transcript per Million mapped reads (FPKM). The Cuffdiff program[131] was then used to compare and identify differentially expressed genes between the Scr and KD conditions.

2.2.8 Protein expression

Enzyme-linked immunosorbent assays (ELISAs) were used to quantify the secreted levels of OPN and OPG in the cell culture media of PiT-2 Scr and KD VSMCs. As serum FBS normally supplemented in growth media can skew ELISA results, serum FBS concentrations were reduced prior to collection of the cell culture media.

PiT-2 Scr and KD VSMCs were treated with DMEM with 1% FBS 24 hours after siRNA treatment. After 24 hours, the medium was replaced with DMEM with 0.5% FBS for 2 days before collection of cell culture media for ELISA. The mouse OPN DuoSet ELISA kit and the mouse OPG Quantikine ELISA kit were used to measure the secreted levels of OPN and OPG respectively, according to the manufacturer's protocol.

2.2.9 Generation of PiT-2 ΔSM mouse

All mouse work was performed with prior IACUC approval and in accordance with policies from the University of Washington. Mice are maintained in a specific pathogen free facility at the University of Washington.

C57BL/6NTac-Slc20a2<tm1a(EUCOMM)Wtsi>/Ieg mice heterozygous for the non-functional knockout first PiT-2 allele was purchased from the European Mutant Mouse Archive. The knockout first allele has a trapping cassette flanked by two FRT sites that disrupts PiT-2 gene function (Fig. 2A). The FRT-flanked region was removed when FLP recombinase was introduced, generating a conditional allele (Fig. 2B) with loxP sites flanking exon 4 of the PiT-2

gene (PiT-2 fl/fl). The region flanked by loxP sites was subsequently removed by the introduction of an SM22α-Cre recombinase, resulting in a recombined allele without exon 4 (Fig. 2C). A mouse homozygous for this recombined allele will have PiT-2 selectively deleted from tissues that express SM22α (PiT-2 ΔSM).

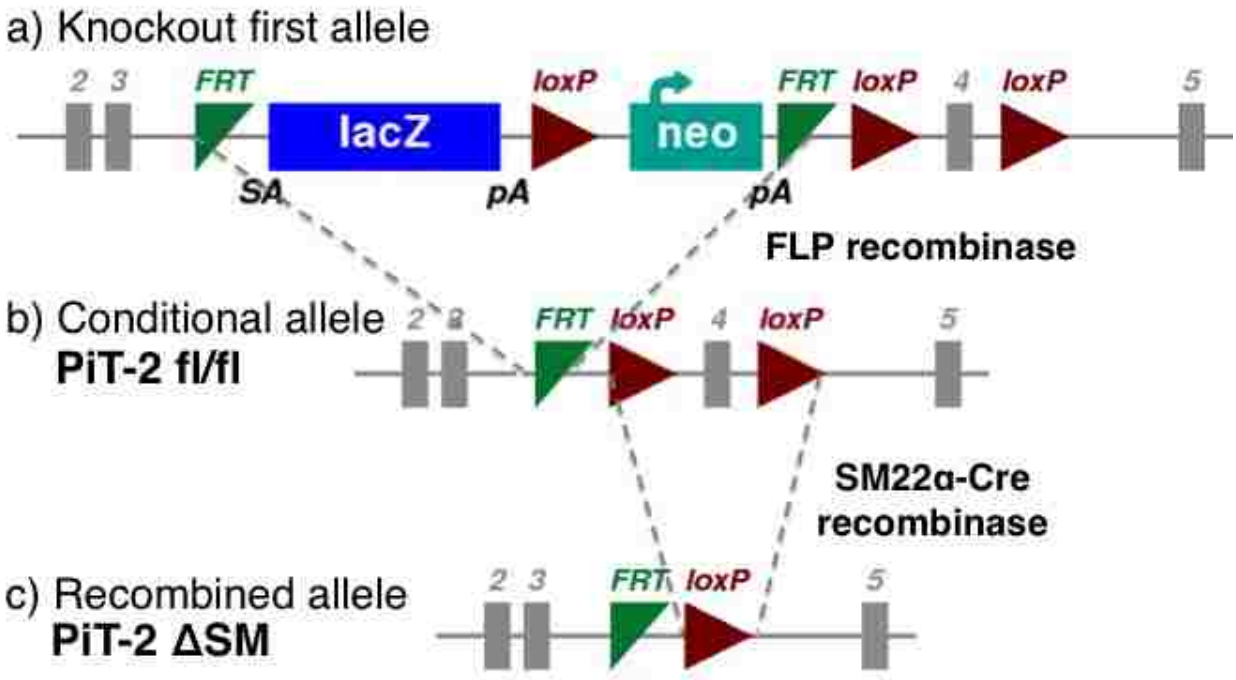

Figure 2: Generation of PiT-2 conditional (fl/fl) and recombined (ΔSM) alleles. A) The knockout first allele has a trapping cassette flanked by two FRT sites that disrupts expression of the PiT-2 gene. B) FLP recombinase removed the FRT-flanked region, generating the conditional allele (PiT-2 fl/fl) and restoring PiT-2 gene function. C) To remove PiT-2 specifically in the VSMCs, an SM22α promoter driven Cre recombinase was used to remove exon 4, flanked by two loxP sites, generating the recombined allele (PiT-2 ΔSM).

2.2.10 Tissue characterization

2.2.10.1 DNA extraction from tissues

For routine genotyping, DNA was extracted from tail clip specimens obtained at weaning using the DNeasy Mini Kit according to the manufacturer's protocol. To confirm genomic DNA rearrangement in the ΔSM transgenic mice, brain surface vessels, thalami, aortas and livers were collected from adult PiT-2 fl/fl and ΔSM mice and immediately snap frozen in liquid nitrogen.

DNA from the respective tissues was extracted using the DNeasy Mini Kit with slight modification. Each tissue sample was incubated in 176 µL of Buffer ATL, 4 µL of 100 mg/mL RNase I solution and 20 µL of Proteinase K. The following table shows the incubation times and elution volumes for each tissue type.

Table 2: DNA extraction from tissues: incubation times and elution volumes

Tissue Type	Incubation Time (hours)	Elution Volume (µL)
Tail	Overnight	100
Aorta	3	50
Brain surface vessels	1	30
Liver	3	100
Thalamus	2	50

2.2.10.2 Genotyping of genomic DNA

100 ng of DNA was loaded on a 0.8% agarose gel containing 0.05% ethidium bromide. The gel was run at 100V for 1 hour, before imaging under UV light. Primers used for genotyping the knockout-first allele[16] are 5'ARM 5'-CAGTAGAACTACCGGAAGGAG-3', 3'ARM 5'-TTGTGCTGCTAGGTGACTGAG-3' and LAR3 5'-CAACGGGTTCTTCTGTTAGT-3'. These primers generated amplicons of 443 bp (knockout first allele) and 523 bp (WT allele). Primers used for genotyping the conditional and recombined alleles are In34F2 5'-CCAAATGCCCAGATAGTTTC-3' and In45R2 5'-CAGCACCTTTCCACAGAGTT-3'. These primers generated amplicons of 1078 bp (WT allele), 1231 bp (conditional allele), and 390 bp (recombined allele). Primers used for genotyping the Cre allele are SMCre.5 5'-CCAAAATTTGCCTGCATTACCGGTCGATGC-3' and SMCre.3 5'-AGCGCCGTAAATCAATCGATGAGTTGCTTC-3', generating an amplicon of 801 bp.

2.2.10.3 Histological preparation of tissues

Mouse whole brains (olfactory bulb removed) and thoracic aortas were collected and fixed in Clark's fixative (3:1 Methanol:Glacial Acetic Acid) for 2 hours on a shaker and stored in 70% ethanol prior to tissue processing. The brains were processed through an ethanol gradient (70%, 95% and 3 changes of 100% for 40 min each), 3 changes of xylenes for 1 hour each, and 2 changes of paraffin at 55°C for 1 hour each. Brains were embedded with the olfactory bulb side down and coronal sections were sectioned 7 μm thick. 5 μm cross sections of the aorta were sectioned made.

2.2.10.4 Alizarin Red S staining

Coronal brain sections from 20-week old PiT-2 fl/fl and ΔSM mice were stained with Alizarin Red S to detect calcium deposits. Coronal brain sections from a 13-week old PiT-2 KO mouse were used as a positive control. Following rehydration of samples by xylene and an ethanol gradient, the sections were then incubated for 1 hour in an Alizarin Red S staining solution at pH 9.0. The sections were destained in a borate buffer containing sodium borate and boric acid at pH 9.0 for 20 seconds, and dehydrated in an ethanol gradient and xylene. Cover slips were mounted with Permount and dried overnight before imaging with a Nikon E800 upright microscope.

2.2.10.5 SM22α immunofluorescence

SM22α immunofluorescence (IF) staining was done on brain coronal sections and aorta cross sections of 20-week old PiT-2 fl/fl and ΔSM mice to qualitatively determine the presence of SM22α in the basal ganglia and thalamus regions and the medial layer of the aorta. Blocking was done with 4% normal donkey serum and 1% BSA in PBS. Antibodies were diluted in 2% normal donkey serum and 1% BSA in PBS. Goat anti-mouse SM22α at 1:500 (1 μg/mL) was

incubated overnight at 4°C. Cy3 AffiniPure Donkey Anti-Goat IgG (H+L) at 1:500 (2.5 μg/mL) was incubated for 30 min at RT. Goat control IgG at 1:1000 (1 μg/mL) was used in place of the primary antibody as a negative control. Cover slips were mounted with ProLong Gold Antifade Mountant and dried overnight before imaging with a Nikon E800 upright microscope.

2.2.11 Cisternal CSF collection and CSF Pi measurement

CSF was collected from the cisterna magna of the mouse brain, as previously described[17,132]. Mice were under anesthesia by isoflurane inhalation during CSF collection. Briefly, glass capillary tubes were pulled on a flaming micropipette puller (heat index = 100, pressure index = 330). Pipette tips were cut such that the inner diameter of the tip was approximately 0.5 mm. CSF was spun down at 2000 RPM for 10 min at 4°C. The supernatant was transferred to a new tube and stored undiluted at 4°C until use. Pi levels in the CSF were measured using the QuantiChrom Phosphate Assay according to the manufacturer's protocols.

2.2.12 Statistics

For comparison of means between two independent groups, a two-tailed Student's t-test with unequal variance was used. For comparison of means in three or more independent groups, a one-way analysis of variance (ANOVA) with a post-hoc Tukey's multiple comparison test was used. Statistical significance was denoted as: ns = $p > 0.05$, * $p < 0.05$, ** $p < 0.01$, *** $p < 0.001$, **** $p < 0.0001$. Data are presented as mean ± standard deviation.

Chapter 3. Results

3.1 PiT-2 haploinsufficiency results in basal ganglia calcification

3.1.1 PiT-2 haploinsufficient mice developed age-dependent BGC

As mutations in the PiT-2 gene are associated with 50% of IBGC cases, we hypothesized that PiT-2 plays a protective role in brain calcification. To this end, mice homozygous (KO) and heterozygous (Het) for the PiT-2 knockout first allele were generated. PiT-2 mRNA expression was measured in whole blood obtained from the saphenous vein of 11-week-old WT, PiT-2 Het and KO mice to confirm the levels of PiT-2. There was an approximately 50% reduction in the Het mice and 99% reduction in the PiT-2 KO mice, compared to the WT controls (Fig. 3A). Alizarin Red S-positive staining of calcium deposits in coronal brain sections confirmed that PiT-2 KO mice developed bilateral BGC in the basal ganglia and thalamic regions[16] (Fig. 3B).

To test the novel hypothesis that PiT-2 haploinsufficient mice develop BGC, coronal brain sections from PiT-2 Het mice were stained with Alizarin Red S as well. These mice developed BGC in an age-dependent manner where Alizarin Red S-positive calcified deposits were minimal at 6 months (Fig. 3C), bilateral at 1 year (Fig. 3D) and prominent at 1.5 years of age (Fig. 3E). This result suggests that PiT-2 haploinsufficiency is sufficient to cause BGC. To our knowledge, this is the first study that accurately recapitulates the autosomal dominant feature of human IBGC in a mouse model.

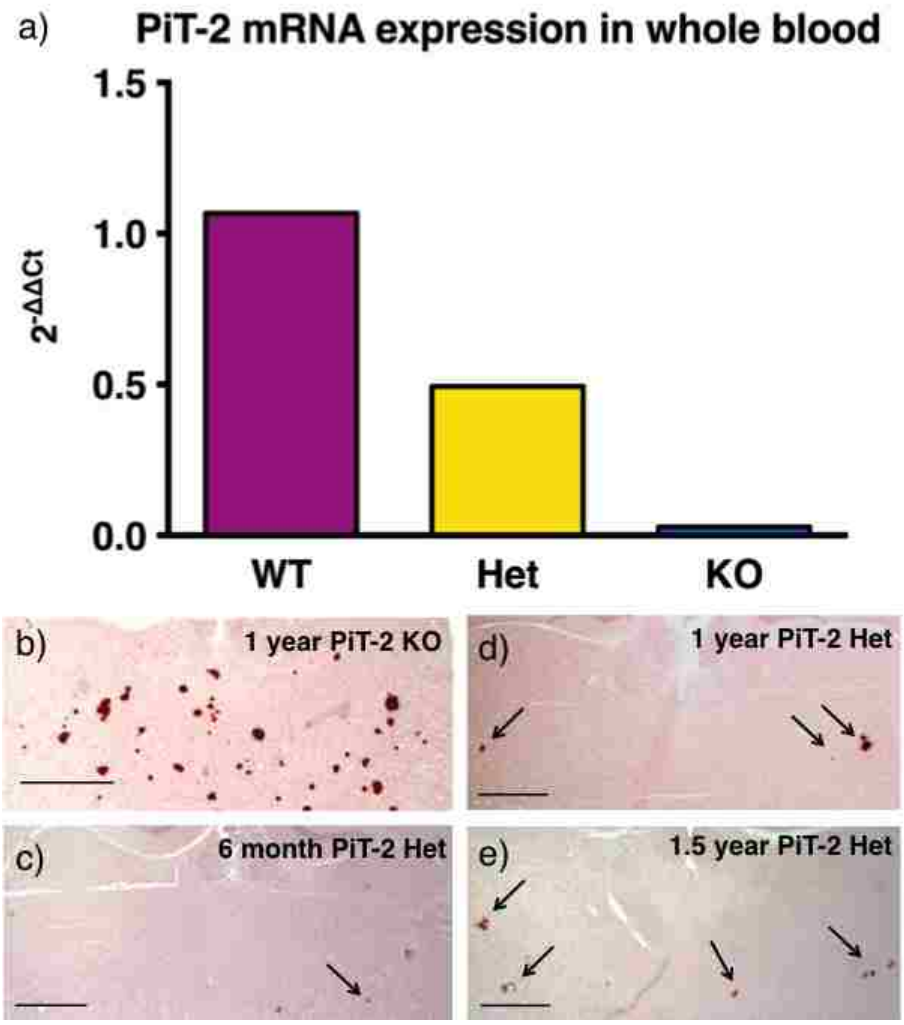

Figure 3: PiT-2 haploinsufficient mice develop BGC. A) PiT-2 Het and KO mice had 50% and 99% reduction of PiT-2 mRNA levels respectively, compared to WT mice (*n*=1). B) Alizarin Red S staining confirmed bilateral BGC in PiT-2 KO mice. C-E) Alizarin Red S-positive calcium deposits (arrows) confirmed age-dependent BGC in PiT-2 Het mice. Scale bar: B-E) 500 μm.

3.1.2 BGC was associated with cerebral arterioles, specifically arteriolar VSMCs

The Alizarin Red S-positive calcified lesions were also positive for von Kossa staining, suggesting that the lesions were composed of calcium phosphate salts (Fig. 4A). Further IF staining found vWF-positive (Fig. 4B) and SMA-positive cells (Fig. 4C) surrounding the calcified lesions, showing that BGC is localized to cerebral arterioles, which is consistent with the findings in an IBGC patient with a mutation in PiT-2[4].

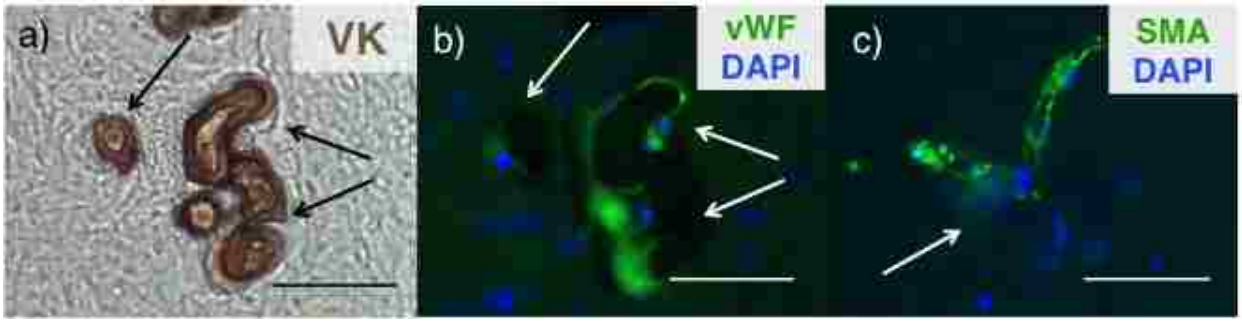

Figure 4: Association of BGC lesions with cerebral arterioles. A) von Kossa-positive staining confirmed that lesions (black arrows) were composed of calcium phosphate salts. B-C) BGC lesions (white arrows) were associated with vWF and SMA-positive cells, characteristic of cerebral arterioles. Scale bar: 50 μm.

The LacZ construct on the PiT-2 knockout first allele (Fig. 2A) provided an additional method to identify PiT-2 expression, by using X-gal staining for β-galactosidase. Coronal brain sections from PiT-2 Het mice showed positive X-gal staining and PiT-2 IF staining colocalizing with SMA-positive cells and was adjacent to glial fibrillary acidic protein (GFAP)-positive astrocytic endfoot processes, confirming that PiT-2 was localized to arteriolar VSMCs (Fig. 5A-F). This suggests that BGC is a form of VC and PiT-2 is required to protect the VSMCs from calcification.

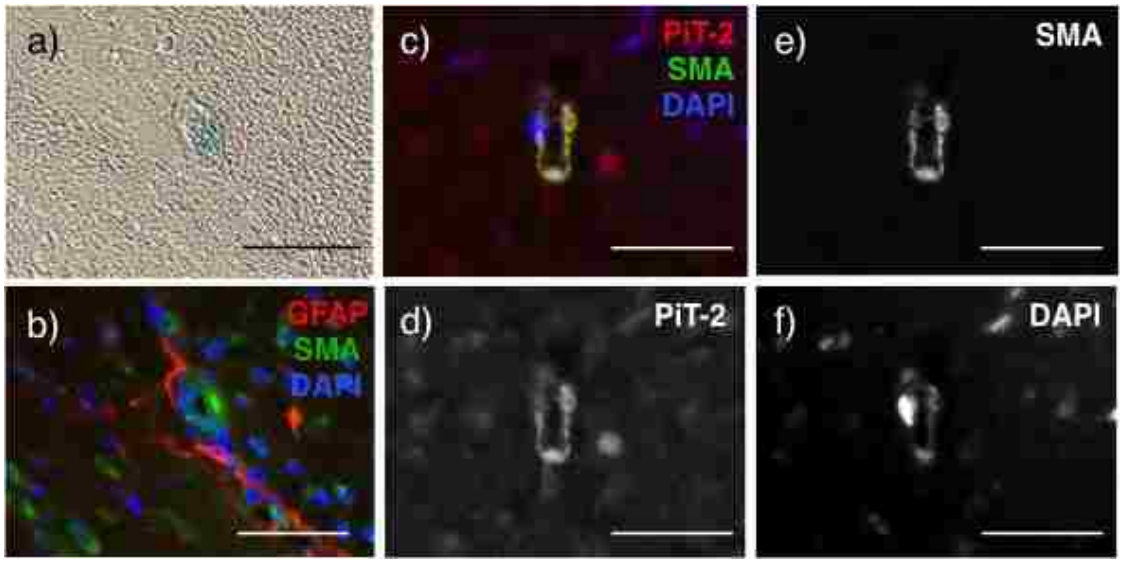

Figure 5: Localization of PiT-2 to arteriolar VSMCs. A-B) X-gal-positive staining for PiT-2 colocalized with SMA-positive cells and is adjacent to GFAP-positive astrocytic endfoot processes. C-F) Positive anti-PiT-2 antibody signal colocalized with SMA-positive cells, confirming PiT-2 expression in arteriolar VSMCs. Scale bar: 50 μm.

3.1.3 PiT-2 was expressed in choroid plexus and ependyma, and required for regulation of CSF Pi levels

In IBGC, the calcification was localized to the brain and not found in the peripheral vasculature. We hypothesized that PiT-2 may be localized to a specialized location in the brain and was specifically involved in protecting the brain vasculature from calcification. Apart from the localization of PiT-2 in cerebral arteriolar VSMCs, the localization of PiT-2 to the choroid plexus (CP) epithelial cells (CP Ep) and the ependyma (Ep) was also investigated. The CP Ep and Ep are involved in CSF production and regulation. Specifically, CP Ep produce CSF, and the Ep is made up of specialized ciliated endothelial-like cells that line the ventricles, providing a barrier between the CSF and the brain. To test this hypothesis, CPs were isolated and the localization of PiT-2 was analyzed. As hypothesized, PiT-2 was strongly expressed in the CP Ep and Ep (Fig. 6A-C). Of note, PiT-2 was localized to the ventricle-facing side of the Ep (Fig. 6A-B), suggesting a potential role of PiT-2 in regulating Pi in the CSF. This hypothesis is further supported by a previous analysis of PiT-2 in spiny dogfish, where PiT-2 was also localized to the apical side of the Ep and involved in actively transporting Pi from the CSF[133]. To test if PiT-2 regulates CSF Pi, CSF was collected from cisterna magna in WT, PiT-2 Het and KO mice, and Pi levels in the CSF were measured using a phosphate assay. There was a significant increase in CSF Pi levels in the KO mice compared to WT mice. The CSF Pi levels in the PiT-2 Het mice were slightly higher than that of the WT mice, but were not significantly different from each other.

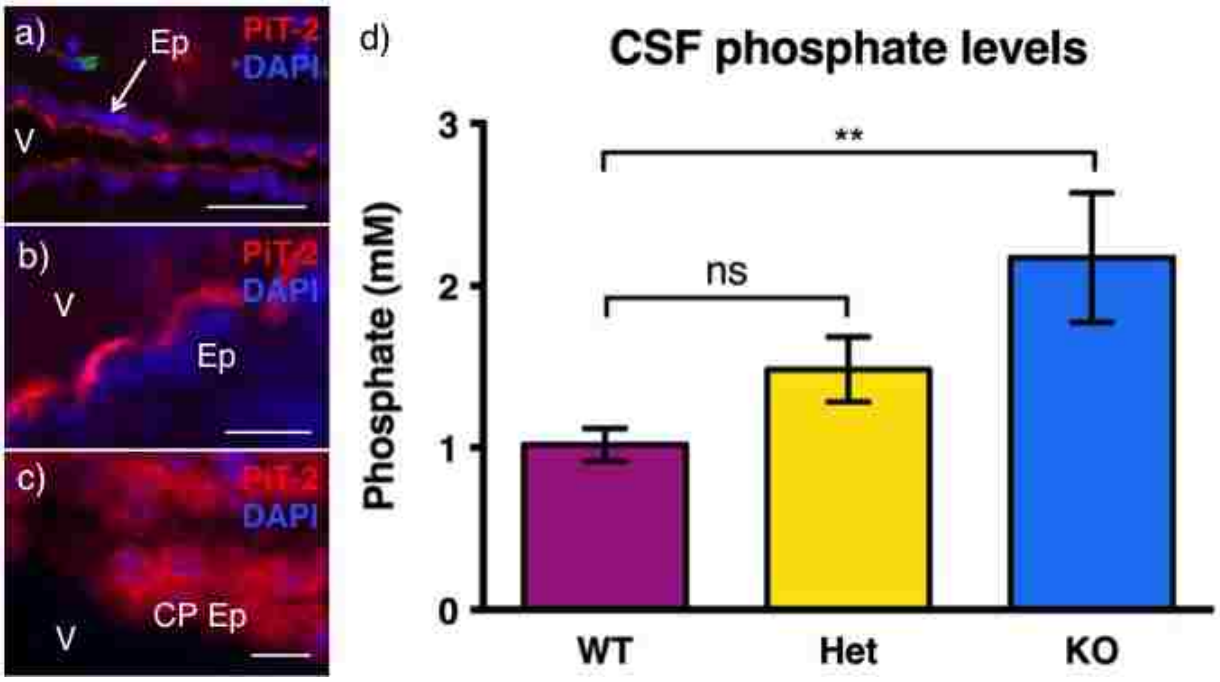

Figure 6: PiT-2 expression in CP Ep and Ep and PiT-2 regulation of CSF Pi levels. A-B) PiT-2 localized to the apical ventricle-facing side of Ep, suggesting Pi is transported out of the CSF. C) CP Ep also showed strong expression of PiT-2. D) CSF Pi levels were trending in the PiT-2 Het mice and significantly increased in the PiT-2 KO mice compared to the WT mice (*n*=3 for WT and KO, *n*=4 for Het). CP Ep: choroid plexus epithelial cells; Ep: ependyma, V: ventricle. Scale bar: A) 50 µm, B-C) 10 µm.

3.2 Role of PiT-2 in VSMCs *in vitro*

3.2.1 siRNA-mediated knockdown of PiT-2 in VSMCs enhanced Pi-induced calcification

A transient PiT-2 knockdown (KD) model was generated using Lipofectamine RNAiMAX liposomal delivery of PiT-2 specific siRNA to cultured WT VSMCs, providing an effective method to study the role of VSMC PiT-2 *in vitro*. PiT-2 specific siRNA was able to reduce PiT-2 mRNA levels by approximately 90% compared to no treatment (NT) and scramble siRNA treated (Scr) control VSMCs, quantified by qPCR (Fig 7A). PiT-1 was also unable to compensate for the loss of PiT-2 expression (Fig. 7B).

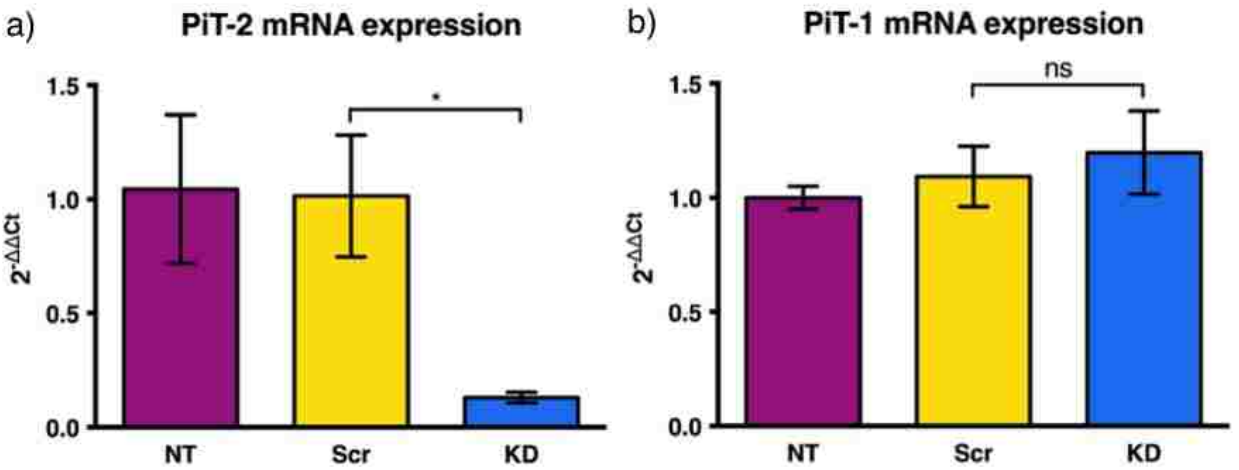

Figure 7: Effect of PiT-2 specific siRNA on WT VSMCs. A) PiT-2 specific siRNA successfully reduced PiT-2 mRNA levels by approximately 90% (*n*=3). B) No compensation in PiT-1 mRNA levels was observed (*n*=3).

Further functional studies showed that PiT-2 KD VSMCs had decreased levels of sodium-dependent Pi uptake (Fig. 8) and increased susceptibility to matrix calcification following treatment with high Pi (2.8 mM) media. Levels of calcification were time-dependent, and were increased approximately two-fold in PiT-2 KD VSMCs compared to Scr VSMCs after 6 days of high Pi treatment (Fig. 9). These findings determined a protective role of PiT-2 in VSMC calcification, consistent with the observation of arteriolar calcification in the brain.

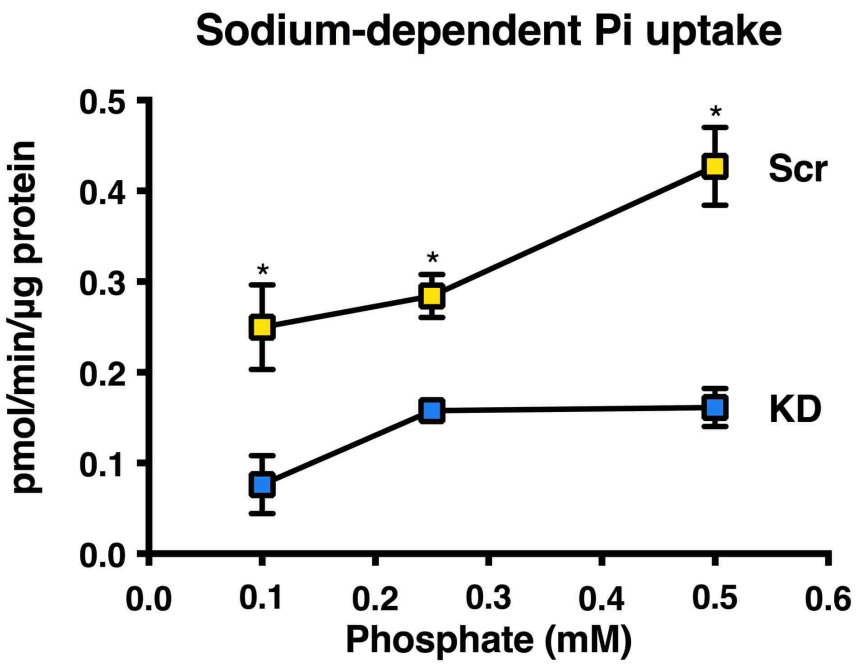

Figure 8: Sodium-dependent Pi uptake levels following PiT-2 KD. PiT-2 KD VSMCs had significantly decreased sodium-dependent Pi uptake levels compared to Scr VSMCs (*n*=3).

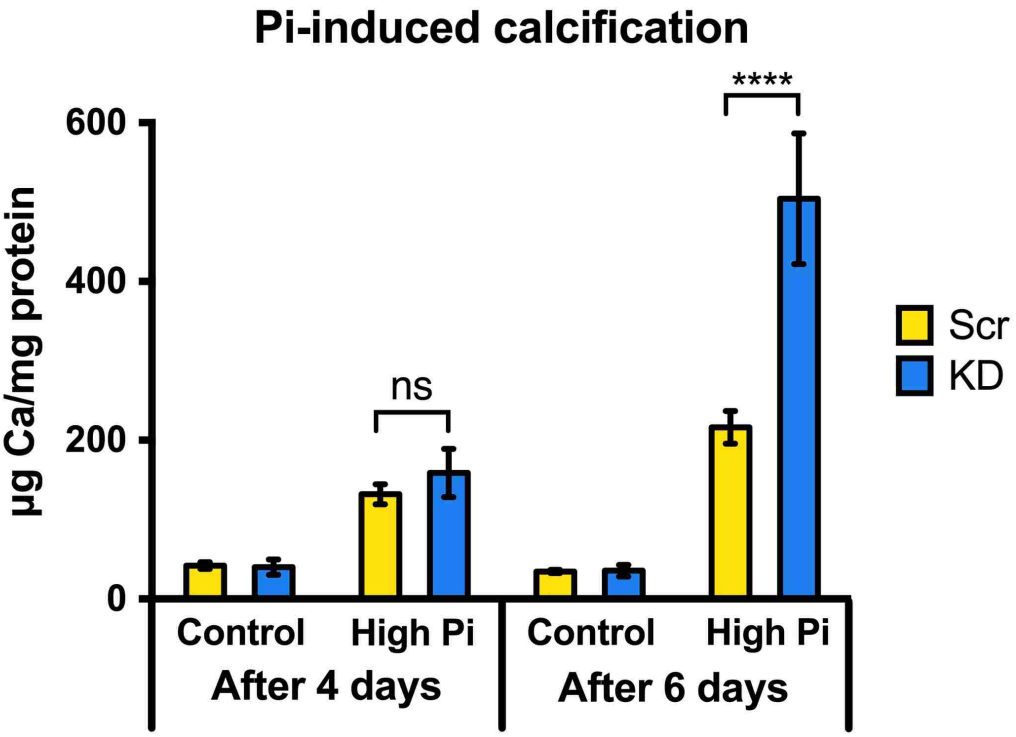

Figure 9: High-Pi induced calcification of PiT-2 VSMCs. Calcification was time-dependent; after 4 days of high Pi media treatment, levels of calcification in PiT-2 Scr and KD VSMCs were not significantly different from each other. After 6 days of high Pi media treatment, PiT-2 KD VSMCs had increased levels of calcification compared to PiT-2 Scr VSMCs (*n*=3).

3.2.2 Reduced secreted PPi levels not observed in PiT-2 deficient VSMCs

To test the hypothesis that reduced PPi levels are associated with VC, secreted PPi levels were measured in VSMC cultures after 6 days of treatment with high Pi (2.8 mM) media. VSMCs cultures treated with normal Pi (0.97 mM) media for the same amount of time were used as controls. The respective culture medium was replaced with Basal Salt Solution and incubated at 37°C for 5 min to allow the secretion of PPi from VSMCs.

PPi was quantified using an enzyme-linked bioluminescence assay, and the bioluminescence was measured with a luminometer. Both the PiT-2 Scr and KD VSMCs treated with high Pi had reduced levels of secreted PPi compared to their respective normal Pi media treatment controls. There was no significant difference in secreted PPi levels between PiT-2 Scr and PiT-2 KD VSMCs treated with high Pi (Fig. 10). This results shows that it is the high Pi treatment, and not the deficiency of PiT-2, that reduced secreted PPi levels – a possible compensatory mechanism in order to maintain Pi/PPi balance.

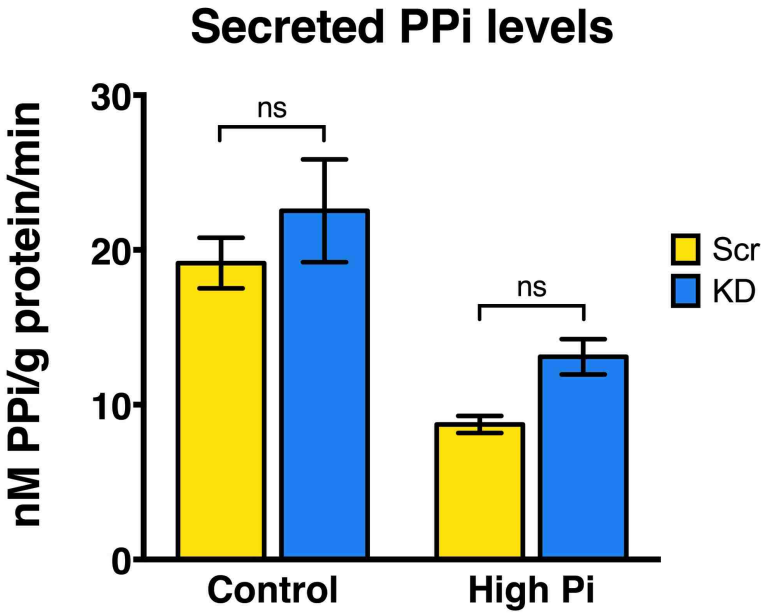

Figure 10: Analysis of secreted PPi levels following PiT-2 KD. There was no significant difference between PiT-2 Scr and KD VSMCs treated with high Pi (n=3).

3.2.3 OC differentiation not observed in PiT-2 deficient VSMCs

OC differentiation is often associated with increased VC, especially with elevated Pi levels, hence the expression of OC-related genes were analyzed following PiT-2 KD. Specifically, RNA was isolated from PiT-2 Scr and KD VSMCs treated with either normal Pi (0.97 mM) or high Pi (2.8 mM) media for 3 days after siRNA treatment, and the expression of SM22α and Runx2 were quantified using qPCR. There was no significant difference in SM22α and Runx2 mRNA expression levels between PiT-2 Scr and KD VSMCs, even with high Pi treatment, suggesting that OC differentiation did not occur following loss of PiT-2 (Fig. 11).

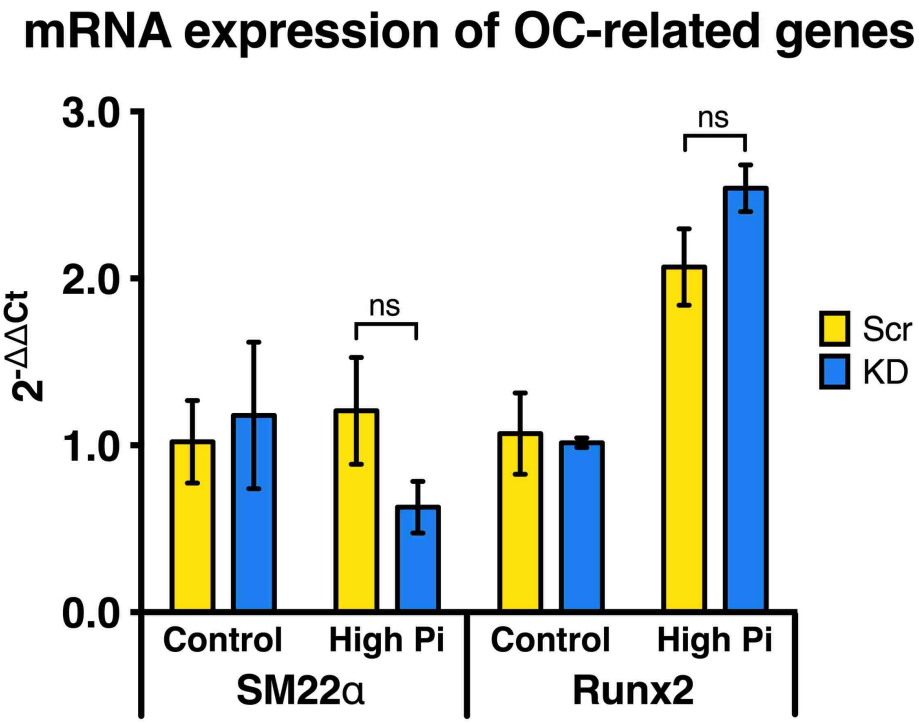

Figure 11: Analysis of OC differentiation following PiT-2 KD. No changes in mRNA expression of SM22α and Runx2 were observed in PiT-2 Scr and KD VSMCs even after high Pi treatment, suggesting that PiT-2 KD does not affect OC differentiation (*n*=3).

3.2.4 Knockdown of PiT-2 reduced production of OPN and OPG

In order to further understand the possible mechanisms underlying PiT-2 protection of VSMC calcification, the expression and secretion of a well-known calcification inhibitor, OPN, were analyzed in PiT-2 Scr and KD VSMCs by qPCR and ELISA respectively. VSMCs treated with high Pi (2.8 mM) media and normal Pi (0.97 mM) media were analyzed to investigate the effects of Pi on the expression and secretion levels of OPN. mRNA expression levels and secreted protein levels of OPN were significantly decreased in the PiT-2 KD VSMCs than in the Scr VSMCs treated with normal Pi media. However, when treated with high Pi media, the PiT-2 KD VSMCs had increased expression and secretion levels of OPN, compared to the respective Scr control (Fig. 12A-B). This increase in expression and secretion levels could possibly be due to a compensatory effect by OPN to inhibit further calcification.

Total RNA sequencing (RNA-Seq) was also carried out, as a quantitative method to identify differentially expressed genes in PiT-2 Scr and KD VSMCs. RNA-Seq identified OPG, another calcification inhibitor, as one of the genes which was differentially expressed in the PiT-2 KD VSMCs compared to the Scr VSMCs (Table 3). qPCR and ELISA confirmed that the expression and secretion levels of OPG were reduced in the PiT-2 KD VSMCs (Fig 12C-D). These results suggest that OPN and OPG may be critical for PiT-2 protection of VSMC calcification.

Table 3 shows the expression levels of several calcification inhibitors in both PiT-2 Scr and KD VSMCs. Both MGP and fetuin A were increased in the PiT-2 KD VSMCs compared to the Scr VSMCs 2 days post-siRNA treatment and to a greater extent after 3 days, which may indicate a possible compensatory event following the loss of PiT-2 and subsequent increase in calcification.

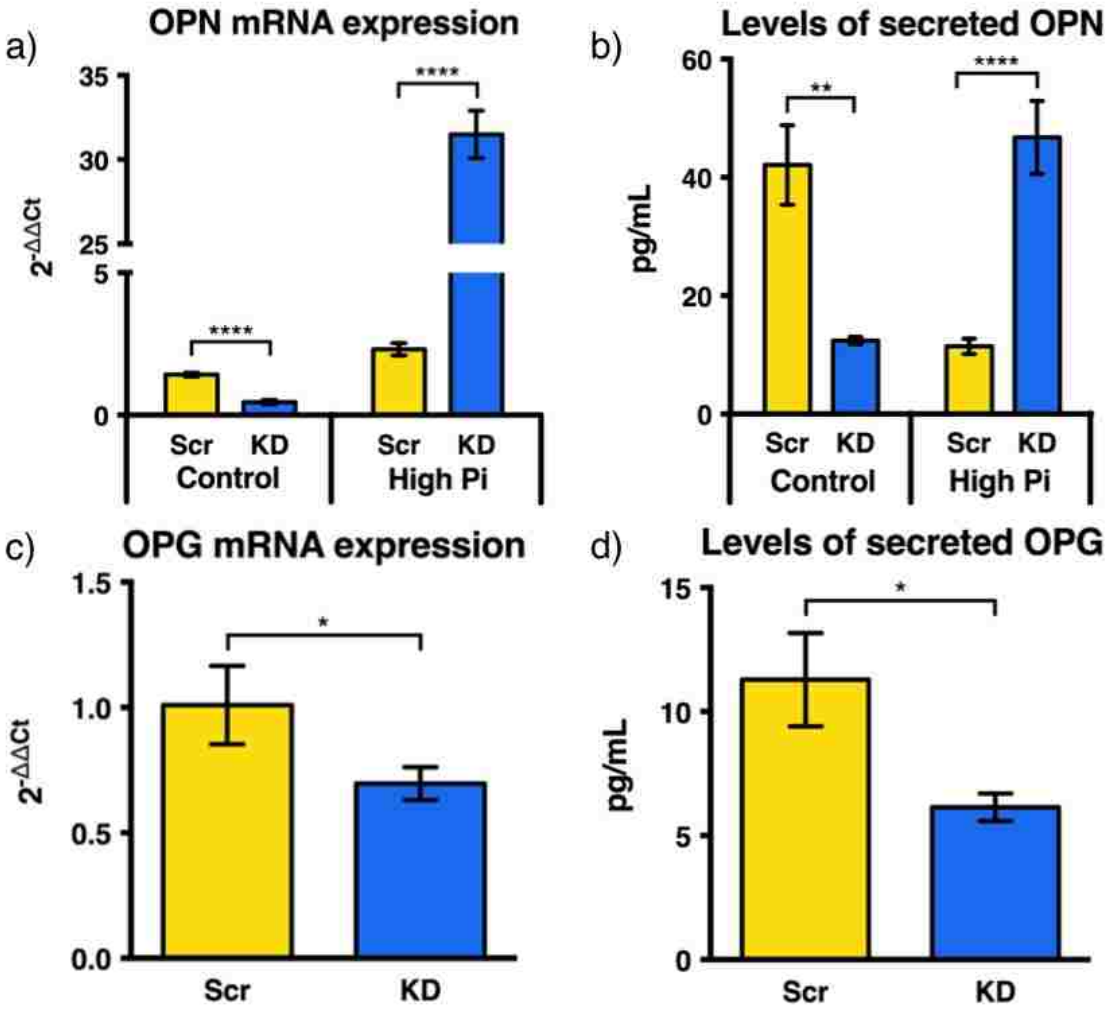

Figure 12: Expression and secretion of calcification inhibitors OPN and OPG following PiT-2 KD. A-B) Expression and secretion levels of OPN, quantified by qPCR and ELISA respectively, were decreased in PiT-2 KD VSMCs (*n*=3). C-D) Expression and secretion levels of OPG, quantified by qPCR and ELISA respectively, were decreased in PiT-2 KD VSMCs (*n*=3).

Table 3: Expression levels of calcification inhibitors identified by RNA-Seq.

	Day 2 post-siRNA treatment			*Day 3 post-siRNA treatment*		
Gene	**Scr (FPKM)**	**KD (FPKM)**	**KD/Scr ratio**	**Scr (FPKM)**	**KD (FPKM)**	**KD/Scr ratio**
MGP	442.48	753.42	1.70	589.32	1334.24	2.26
AHSG (Fetuin A)	0.38	0.57	1.48	0.66	1.26	1.92
OPN	1.21	1.10	0.91	0.82	0.48	0.58
OPG	26.62	14.50	0.54	46.09	18.51	0.40

3.2.5 Knockdown of PiT-2 increased susceptibility of VSMC to cell death

Cell death often leads to calcification, hence the susceptibility of VSMCs to cell death following PiT-2 knockdown was investigated. PiT-2 Scr and KD VSMCs were treated with either normal Pi or high Pi media, and cell death was analyzed with the LIVE/DEAD Cytotoxicity/Viability Kit 2 and 6 days after Pi addition. Live and dead cells in the VSMC cultures were stained with calcein-AM and ethidium homodimer-1 respectively, and quantified by imaging 5 fields of view per biological replicate. PiT-2 Scr and KD VSMCs, regardless of Pi concentration in the media, had similar percentages of dead cells 2 days following Pi treatment. After 6 days of Pi treatment, the percentage of dead cells increased in the high Pi treated VSMCs, and the PiT-2 KD VSMCs had a significantly higher percentage of dead cells compared to the PiT-2 Scr VSMCs (Fig. 13). This result suggests that PiT-2 normally protects VSMCs from calcification by inhibiting cell death, and PiT-2 deficiency results in decreased inhibition, thereby increasing VSMC susceptibility to calcification.

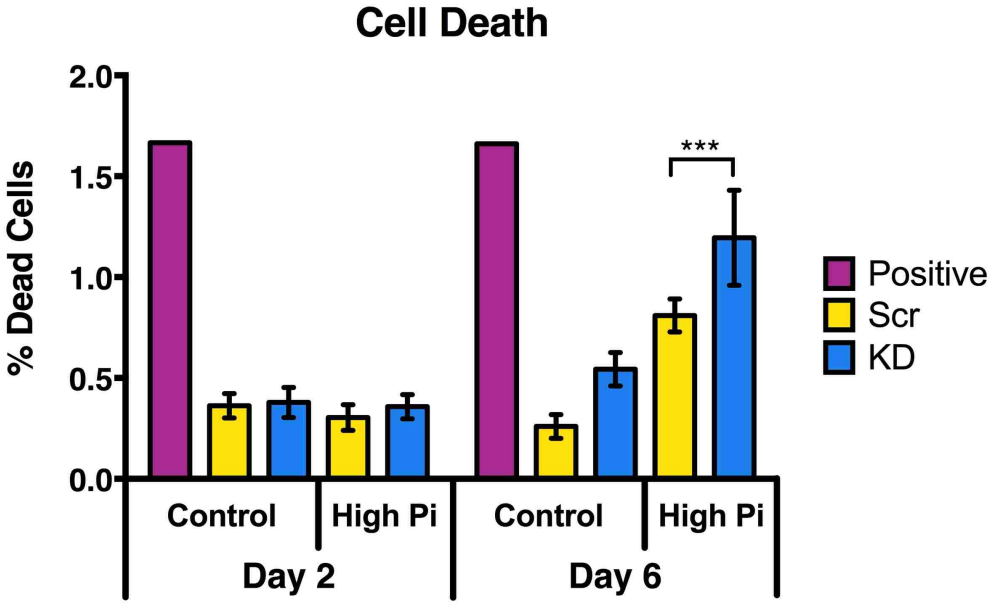

Figure 13: Levels of cell death following PiT-2 KD. PiT-2 KD did not affect cell death after 2 days of Pi treatment. The levels of cell death in PiT-2 KD VSMCs significantly increased after 6 days of Pi treatment (n=4 for Scr and KD, n=1 for positive control).

3.3 Characterization of PiT-2 ΔSM mouse model

3.3.1 SM22α-Cre recombinase mediated genomic DNA rearrangement of conditional PiT-2 alleles

In order to analyze SM22α-Cre mediated genomic DNA rearrangement of the conditional PiT-2 alleles, brain surface vessels, thalami, and aortas were isolated from PiT-2 fl/fl and ΔSM mice. Livers were used a negative control. Primers specific to the sequence prior to the floxed exon 4 region identified the conditional allele in all the PiT-2 fl/fl and ΔSM tissues (Fig. 14A). The presence of Cre was detected in only the PiT-2 ΔSM tissues that contained the SM22α-Cre allele (Fig. 14B). Primers that amplify a sequence in the floxed exon 4 region determined that exon 4 was effectively deleted in the brain surface vessels, thalamus, and aorta from the PiT-2 ΔSM mice. There was no SM22α-Cre mediated DNA rearrangement in the fl/fl tissues and very minimal rearrangement detected in the PiT-2 ΔSM liver, as the liver is a highly vascularized organ. There were also several non-specific bands, most likely due to the presence of PiT-2 in other cell types in contaminating tissue that could not been avoided during tissue collection (Fig. 14C).

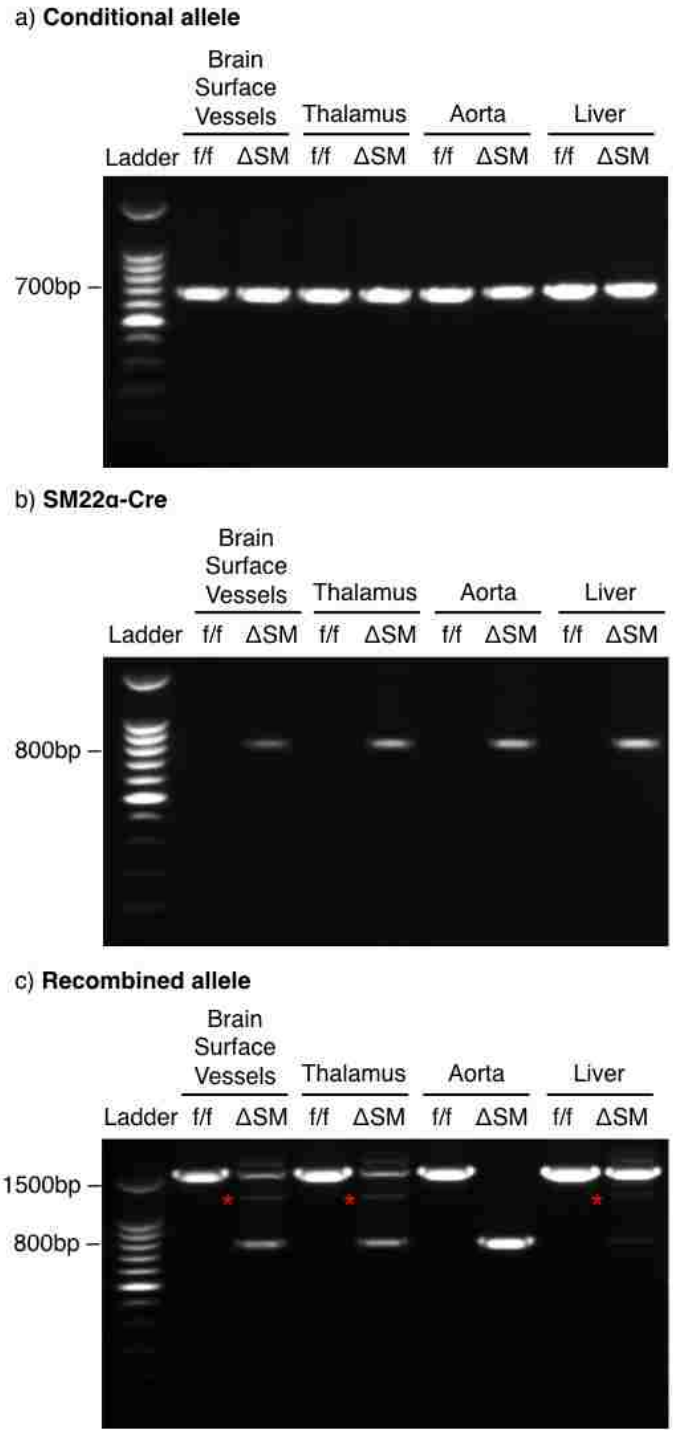

Figure 14: Genomic DNA arrangement of PiT-2 conditional allele. A) The conditional allele was identified PiT-2 fl/fl and ΔSM tissues. Expected band size: 633bp. B) The presence of Cre-recombinase was only detected in ΔSM tissues. Expected band size: 801 bp. C) SM22α-Cre mediated DNA rearrangement of the conditional allele in ΔSM tissues. Contaminating tissue contributed to the non-specific bands (red asterisks). Expected band size: 776bp.

3.3.2 SM22α expressed in VSMCs in the aorta, basal ganglia and thalami

IF staining was used to detect the presence of SM22α in the aortas, basal ganglia and thalami of 20-week old PiT-2 fl/fl and ΔSM mice, to confirm the ability of the SM22α-Cre recombinase to mediate the recombination of the conditional allele. SM22α expression was observed specifically in the VSMCs of the aortas, and the vessels of the brains in both the PiT-2 fl/fl and ΔSM mice (Fig. 15).

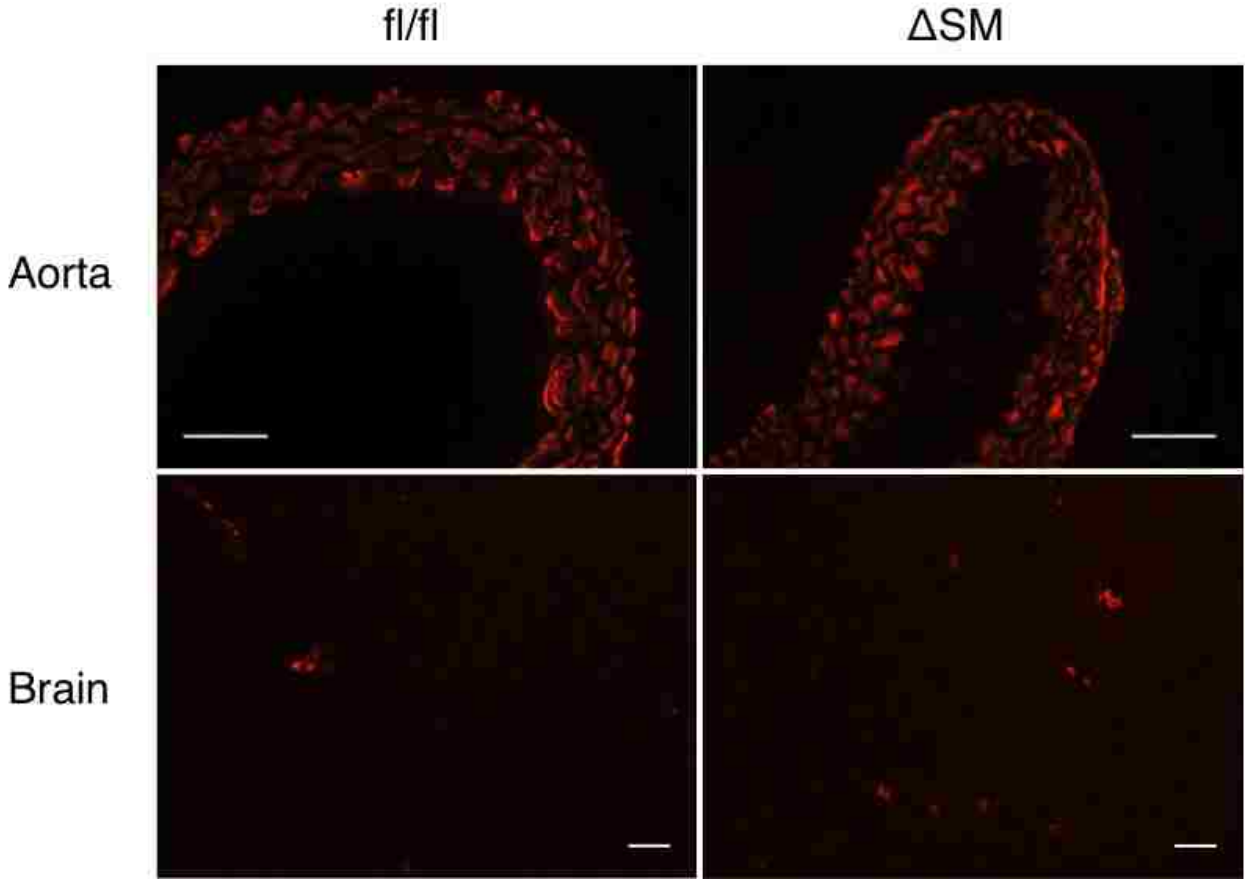

Figure 15: SM22α IF staining in aorta and brain of PiT-2 fl/fl and ΔSM mice. SM22α was specifically detected in the VSMCs of the aortas, and in the vessels of the basal ganglia and thalamus regions of both PiT-2 fl/fl and ΔSM mice. Scale bar: 50 μm.

3.3.3 PiT-2 ΔSM mice did not develop BGC

To understand if the deletion of PiT-2 specifically in VSMCs results in BGC, coronal brain sections from 20-week old PiT-2 fl/fl and ΔSM mice were stained for calcium with Alizarin Red S. No calcium deposits were identified in the basal ganglia or the thalami of the PiT-2 fl/fl and ΔSM brains (Fig. 16), suggesting that PiT-2 deletion in VSMCs alone does not result in BGC.

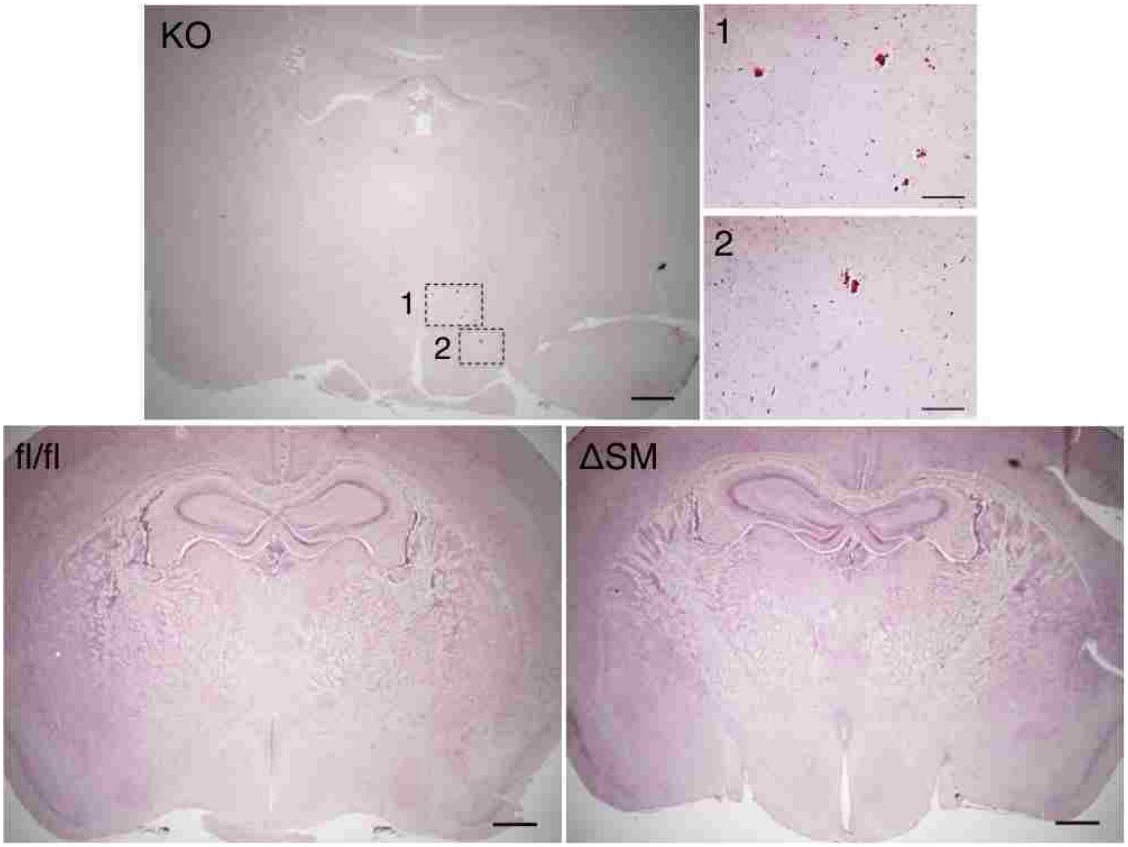

Figure 16: Alizarin Red S staining in brain coronal sections. Calcium deposits were not identified in brains from 20-week old PiT-2 fl/fl and ΔSM mice. 2 PiT-2 fl/fl mice and 5 ΔSM mice were analyzed, and representative images are shown. A 13-week old PiT-2 KO brain was used as a positive control and calcium deposits were identified in the basal ganglia. Scale bar: KO, fl/fl, ΔSM) 500 µm, 1, 2) 50 µm.

3.3.4 Knockout of PiT-2 in VSMCs did not alter CSF Pi levels

The PiT-2 global KO mice had increased levels of Pi in the CSF, suggesting that PiT-2 played a role in the regulation of CSF Pi. To investigate whether VSMC-specific deletion of PiT-

2 resulted in altered CSF Pi levels, CSF was collected from the cisterna magna of 20-week old PiT-2 fl/fl and ΔSM mice and Pi levels were measured using a phosphate assay. CSF Pi levels in the PiT-2 ΔSM mice were not significantly different from that of the PiT-2 fl/fl mice (Fig. 17), suggesting that VSMC PiT-2 alone does not play a role in regulating CSF Pi.

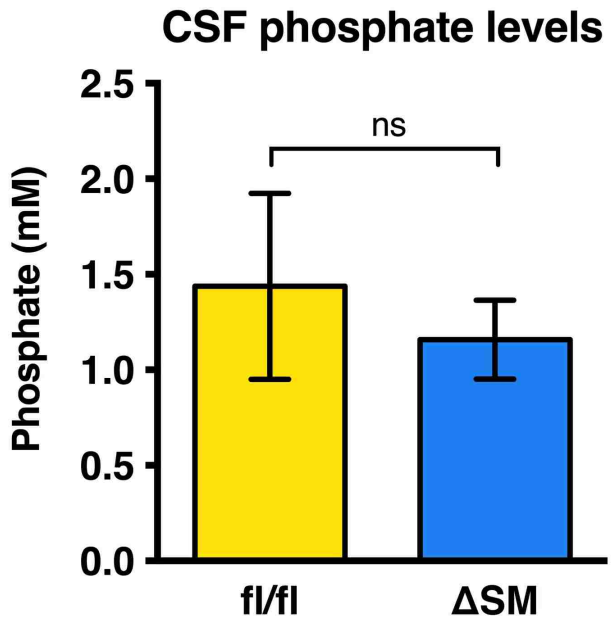

Figure 17: Analysis of CSF Pi levels. Pi was measured in CSF collected from PiT-2 fl/fl and ΔSM mice. CSF Pi levels of PiT-2 ΔSM mice were not significantly different from that of PiT-2 fl/fl mice (*n*=3).

Chapter 4. Conclusion and Future Work

4.1 Summary and Conclusion

This research study focused on PiT-2 in VSMCs, and investigated the mechanisms underlying its role in protecting the VSMCs from calcification. To this end, an siRNA-mediated PiT-2 knockdown model in VSMCs was developed. siRNA-mediated KD of PiT-2 reduced Pi uptake levels but resulted in increased susceptibility to Pi-induced calcification, suggesting that PiT-2 is protective against calcification. Using this *in vitro* model, several mechanisms of VC were investigated, including secreted PPi levels, OC differentiation, inhibitors of calcification, and cell death. PiT-2 KD in VSMCs did not significantly alter secreted PPi or promote OC differentiation, ruling out these two mechanisms as potential causes of the increased VSMC calcification observed. On the other hand, PiT-2 deficiency resulted in the decreased expression and secretion of two well-known calcification inhibitors, OPN and OPG, as well as increased levels of cell death. These results suggested that PiT-2 in VSMCs could be involved in preventing VSMC calcification by normally maintaining high levels of calcification inhibitors such as OPN and OPG, and also by inhibiting cell death.

Previous studies from our lab have investigated the role of PiT-2 *in vivo* by generating the PiT-2 Het and KO mice and found that haploinsufficiency of PiT-2 was sufficient to cause BGC[17]. This was the first animal model that successfully recapitulated the autosomal dominant feature of human IBGC. PiT-2 Het and KO mice developed calcified lesions associated with cerebral arterioles in the basal ganglia and thalamic regions. In addition to VSMCs, PiT-2 was also highly expressed in the CP Ep and Ep. The lack of PiT-2, especially in these tissues, resulted in increased CSF Pi levels.

In order to supplement the *in vitro* findings hypothesizing that PiT-2 played a role in protecting VSMCs from Pi-induced calcification, a VSMC-specific PiT-2 knockout model was developed for this study. PiT-2 was successfully deleted from the VSMCs, as confirmed by DNA rearrangement in brain surface vessels, thalami and aortas. IF staining in the brain and the aorta of PiT-2 fl/fl and ΔSM mice also revealed that SM22α was present in the VSMCs of the aortas and the vessels of the brains, suggesting that the SM22α Cre mediated the recombination of the conditional allele. However, PiT-2 ΔSM mice did not develop calcified lesions in the brain or have altered CSF Pi levels, compared to the PiT-2 fl/fl mice. These results suggest that the removal of PiT-2 in the VSMCs alone is insufficient to cause BGC that was observed in the PiT-2 global KO mice.

These findings point towards a two-hit mechanism underlying BGC. Under normal conditions, PiT-2 in the CP Ep, Ep and cerebral VSMCs adjacent to CSF-containing spaces maintains normal levels of Pi in the CSF (Fig. 18A-D). In this case, VSMC PiT-2 plays a role in regulating CSF Pi levels, specifically by transporting Pi out of the CSF in the glymphatic space, and thereby protecting VSMCs against calcification. However, when PiT-2 is deficient in these cells, Pi concentration in CSF increases. Concomitant with the lack of Pi clearance from the CSF due to the absence of PiT-2, the accumulation of Pi in CSF in the glymphatic spaces surrounding the cerebral VSMCs provides a localized high Pi environment that initiates VSMC calcification and plays a role in the development of BGC (Fig. 18E-H). Both the lack of PiT-2 expression and the presence of a high Pi environment are required for the initiation and development of BGC.

This study provided a deeper understanding of PiT-2 in IBGC and uncovered its novel role in preventing VSMC calcification. It not only elucidated the potential mechanisms by which

PiT-2 demonstrates its protective role, but also provided an insight into potential therapeutic targets for patients with IBGC and other diseases that also result in BGC.

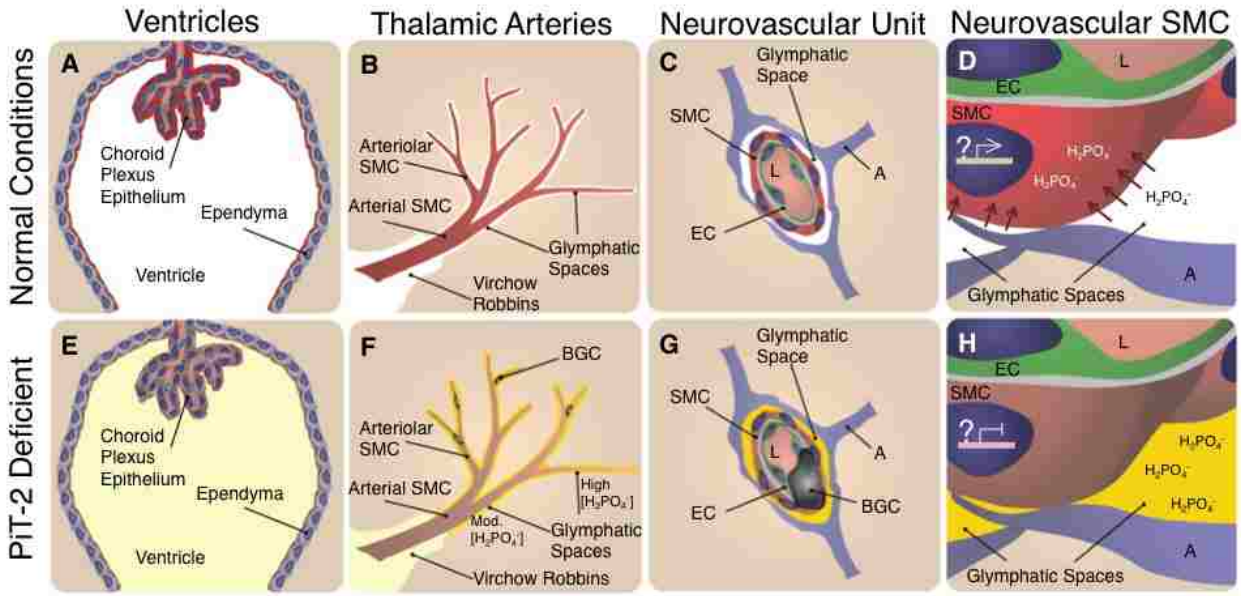

Figure 18: Summary of proposed two-hit mechanism underlying BGC. A-D) Under normal conditions, PiT-2 in CSF-adjacent tissues like Cp Ep, Ep and VSMCs maintains normal Pi levels in the CSF. E-H) PiT-2 deficiency leads to lack of Pi clearance, thereby leading to Pi accumulation and increased Pi levels in the CSF. As a result of being exposed to a high Pi environment, VSMCs calcify and results in BGC. A: Astrocyte, BGC: basal ganglia calcification, EC: endothelial cell, L: lumen, SMC: smooth muscle cell.

4.2 Future work

This study has presented the novel protective role of PiT-2 in VSMCs, evaluated the mechanisms that may underlie IBGC, and generated a VSMC-specific PiT-2 knockout model. Possible future work for this study include:

4.2.1 Pi uptake-independent mechanisms of PiT-2

Pi uptake-independent signaling mechanisms of PiT-1 that promote VSMC calcification were recently identified[44]. However, whether PiT-2 protects VSMCs from calcification through Pi uptake-dependent or -independent pathways has not been elucidated. In our study, PiT-2 KD VSMCs had reduced Pi uptake levels, but had increased levels of calcification, suggesting there

are Pi uptake-independent mechanisms that may promote calcification as well. In an elegant study by Wang *et al.*, seven novel mutations linking IBGC to Pi homeostasis in the human PiT-2 gene were identified. Expressing these mutations in *Xenopus* laevis oocytes significantly impacted Pi uptake levels. The ability of these mutants to calcify was not evaluated. The mouse equivalents of the human PiT-2 mutations could be generated and introduced into mouse VSMCs, generating transport deficient mutant VSMCs. To evaluate if the protective role of PiT-2 is mediated through Pi uptake-dependent or -independent pathways, the levels of calcification in the transport deficient mutants can be assessed. To further understand the mechanisms involved, levels of cell death and inhibitors such as OPN and OPG can also be measured in these mutants.

4.2.2 Regulation of PiT-2

Currently, what regulates PiT-2 is unknown. Two potential regulators include PDGFB and PTH. Mutations in PDGFB and PDGFRB also result in IBGC, although to a lesser extent than PiT-2. PDGF is a potent growth factor for cells with mesenchymal origins, including VSMCs. Specifically, PDGF stimulation of VSMCs can result in cell migration, proliferation, angiogenesis, and apoptosis[134–137]. PDGF has also been shown to increase expression of PiT-2[138] and Pi uptake in fibroblast[139–141], although its relation to ectopic calcification is undetermined. It is a possible that reduced signaling of PDGF leads to a decreased expression of PiT-2, thereby reducing protection from VSMC calcification and IBGC. PTH is a key hormone that regulates serum levels of calcium and Pi, as detailed in Section 1.3.6. PTH is also linked to secondary BGC, which is radiologically indistinguishable from IBGC and occurring in 70-80% of hypoparathyroidism cases. PTH has also been shown to regulate PiT-1 expression in HEK-293 cells[142]. It is currently unknown whether PTH affects PiT-2, Pi transport or VSMC calcification.

Conversely, PiT-2 could regulate PDGFB. Since mutations in PDGFB and PDGFRB also lead to IBGC, the loss of PiT-2 may reduce PDGF signaling thereby leading to calcification. Since serum PTH levels in IBGC patients are generally normal, it is unlikely that PiT-2 regulates PTH. However, it is possible that even though serum PTH levels are normal, there could be an impaired ability of PTH to stimulate PiT-2 in VSMCs, resulting in less inhibition of calcification.

Understanding regulators of PiT-2 could be helpful in developing therapeutics to target IBGC. Even if a specific cell type is identified as the cell type responsible for IBGC, direct delivery of exogenous PiT-2 to that cell type may prove difficult. Apart from requiring the molecule to bypass blood brain barrier, further engineering of the PiT-2 protein is required to allow the protein to localize to the membrane. Therefore, a regulator upstream of PiT-2 could serve as a target for IBGC treatment instead.

4.2.3 Generation of ciliated epithelial cell-specific PiT-2 knockout model

This study generated VSMC-specific knockout mice to study the role of VSMC PiT-2 on BGC. It has been suggested that PiT-2 in the Cp Ep and Ep also plays a role in the development of BGC. To understand the role of Cp Ep and Ep PiT-2, ciliated epithelial cell-specific knockout mice using a Foxj1-driven Cre recombinase can be generated. Similar characterization and analysis of brain calcification can be done to determine if Cp Ep and Ep PiT-2 are involved in BGC. In addition, an SM22α-Cre and Foxj1-Cre specific double knockout of PiT-2 can also be generated to evaluate our two-hit hypothesis underlying the development of BGC.

List of References

1. Mufaddel, A. A. & Al-Hassani, G. A. Familial idiopathic basal ganglia calcification (Fahr`s disease). *Neurosciences (Riyadh)*. **19,** 171–7 (2014).

2. Manyam, B. V., Walters, A. S. & Narla, K. R. Bilateral Striopallidodentate calcinosis: Clinical characteristics of patients seen in a registry. *Mov. Disord.* **16,** 258–264 (2001).

3. Duckett, S., Galle, P., Escourolle, R., Poirier, J. & Hauw, J. J. Presence of zinc, aluminum, magnesium in striopalledodentate (SPD) calcifications (Fahr's disease): Electron probe study. *Acta Neuropathol.* **38,** 7–10 (1977).

4. Kimura, T. *et al.* Familial idiopathic basal ganglia calcification: Histopathologic features of an autopsied patient with an SLC20A2 mutation. *Neuropathology* (2015). doi:10.1111/neup.12280

5. Yamada, M. *et al.* High frequency of calcification in basal ganglia on brain computed tomography images in Japanese older adults. *Geriatr. Gerontol. Int.* **13,** 706–710 (2013).

6. Simoni, M. *et al.* Prevalence of CT-detected cerebral abnormalities in an elderly Swedish population sample. *Acta Neurol. Scand.* **118,** 260–267 (2008).

7. Nicolas, G. *et al.* Phenotypic spectrum of probable and genetically-confirmed idiopathic basal ganglia calcification. *Brain* **136,** 3395–3407 (2013).

8. Wang, C. *et al.* Mutations in SLC20A2 link familial idiopathic basal ganglia calcification with phosphate homeostasis. *Nat Genet* **44,** 254–256 (2012).

9. de Oliveira, D. F., de Lemos, R. R. & de Oliveira, J. R. Mutations at the SLC20A2 gene and brain resilience in families with idiopathic basal ganglia calcification ('Fahr's disease'). *Front Hum Neurosci* **7,** 420 (2013).

10. Saleem, S. *et al.* Fahr's syndrome: literature review of current evidence. *Orphanet J. Rare Dis.* **8,** 156 (2013).

11. Zhang, Y., Guo, X. & Wu, A. Association between a novel mutation in SLC20A2 and familial idiopathic basal ganglia calcification. *PLoS One* **8,** e57060 (2013).

12. Nicolas, G. *et al.* Brain calcification process and phenotypes according to age and sex: Lessons from SLC20A2, PDGFB, and PDGFRB mutation carriers. *Am. J. Med. Genet. B. Neuropsychiatr. Genet.* **168,** 586–594 (2015).

13. Legati, A. *et al.* Mutations in XPR1 cause primary familial brain calcification associated with altered phosphate export. *Nat. Genet.* **47,** 579–581 (2015).

14. Moura, D. A. P. & Oliveira, J. R. M. XPR1: a Gene Linked to Primary Familial Brain Calcification Might Help Explain a Spectrum of Neuropsychiatric Disorders. *J. Mol. Neurosci.* **57,** 519–521 (2015).

15. Hsu, S. C. *et al.* Mutations in SLC20A2 are a major cause of familial idiopathic basal ganglia calcification. *Neurogenetics* **14,** 11–22 (2013).

16. Jensen, N. *et al.* Loss of function of slc20a2 associated with familial idiopathic Basal Ganglia calcification in humans causes brain calcifications in mice. *J Mol Neurosci* **51,** 994–999 (2013).

17. Wallingford, M. *et al.* SLC20A2 deficiency in mice leads to elevated phosphate levels in cerbrospinal fluid and glymphatic pathway-associated arteriolar calcification, and recapitulates human idiopathic basal ganglia calcification. *Brain Pathol.* **3,** [Epub ahead of print] (2016).

18. Speer, M. Y. *et al.* Smooth muscle cells give rise to osteochondrogenic precursors and chondrocytes in calcifying arteries. *Circ. Res.* **104,** 733–741 (2009).

19. Wada, T., McKee, M. D., Steitz, S. & Giachelli, C. M. Calcification of vascular smooth muscle cell cultures: inhibition by osteopontin. *Circ. Res.* **84,** 166–178 (1999).

20. Trion, A. & Van Der Laarse, A. Vascular smooth muscle cells and calcification in atherosclerosis. *American Heart Journal* **147,** 808–814 (2004).

21. Mizobuchi, M., Towler, D. & Slatopolsky, E. Vascular calcification: the killer of patients with chronic kidney disease. *J Am Soc Nephrol* **20,** 1453–1464 (2009).

22. Basak, R. C. A case report of Basal Ganglia calcification - a rare finding of hypoparathyroidism. *Oman Med. J.* **24,** 220–2 (2009).

23. Brannan, T. S., Burger, a a & Chaudhary, M. Y. Bilateral basal ganglia calcifications visualised on CT scan. *J. Neurol. Neurosurg. Psychiatry* **43,** 403–6 (1980).

24. Dai, X. *et al.* Identification of a novel genetic locus on chromosome 8p21.1-q11.23 for idiopathic basal ganglia calcification. *Am J Med Genet B Neuropsychiatr Genet* **153b,** 1305–1310 (2010).

25. Lazar, M., DA, I., Streinu-Cercel, A. & AI, B. Fahr's syndrome: diagnosis issues in patients with unknown family history of disease. *Rom J Morphol Embryol* **50,** 425–428 (2009).

26. Wider, C., Dickson, D. W., Schweitzer, K. J., Broderick, D. F. & Wszolek, Z. K. Familial idiopathic basal ganglia calcification: a challenging clinical-pathological correlation. *Journal of neurology* **256,** 839–842 (2009).

27. Wang, C. *et al.* Molecular mechanism of idiopathic basal ganglia calcification. *Hered.* **37,** 731–740 (2015).

28. Pan, B. *et al.* Idiopathic basal ganglia calcification presenting as schizophrenia-like psychosis and obsessive-compulsive symptoms: A case report. *Exp. Ther. Med.* **10,** 608–610 (2015).

29. Yang, C.-S., Lo, C.-P. & Wu, M.-C. Ischemic stroke in a young patient with Fahr's disease: a case report. *BMC Neurol.* **16,** 33 (2016).

30. Wityk, R. J., Lapeyrolerie, D. & Stein, B. D. Rapid Brain Calcification after Ischemic Stroke. *Ann. Intern. Med.* **119,** 490–491 (1993).

31. Chen, X., Lam, W. W. M., Ng, H. K., Fan, Y. & Wong, K. S. Intracranial artery calcification: a newly identified risk factor of ischemic stroke. *J. Neuroimaging* **17,** 300–3 (2007).

32. Bugnicourt, J. M. *et al.* High prevalence of intracranial artery calcification in stroke patients with CKD: A retrospective study. *Clin. J. Am. Soc. Nephrol.* **4,** 284–290 (2009).

33. Sobrido, M. J., Coppola, G., Oliveira, J. R. M., Hopfer, S. & Geschwind, D. H. in *GeneReviews [Internet]* (eds. Pagon, R. A., Adam, M. P. & Ardinger, H. H.) (2016).

34. Koller, W. C., Cochran, J. W. & Klawans, H. L. Calcification of the basal ganglia: computerized tomography and clinical correlation. *Neurology* **29,** 328–33 (1979).

35. Harrington, M. G., Macpherson, P., McIntosh, W. B., Allam, B. F. & Bone, I. The significance of the incidental finding of basal ganglia calcification on computed tomography. *J. Neurol. Neurosurg. Psychiatry* **44,** 1168–70 (1981).

36. Forstl, H., Krumm, B., Eden, S. & Kohlmeyer, K. Neurological disorders in 166 patients with basal ganglia calcification: a statistical evaluation. *J Neurol* **239,** 36–38 (1992).

37. Manyam, B. V. What is and what is not 'Fahr's disease'. *Park. Relat. Disord.* **11,** 73–80 (2005).

38. Rosenblatt, A. & Leroi, I. Neuropsychiatry of Huntington's disease and other basal ganglia disorders. *Psychosomatics* **41,** 24–30 (2000).

39. Shouyama, M., Kitabata, Y., Kaku, T. & Shinosaki, K. Evaluation of regional cerebral blood flow in Fahr disease with schizophrenia-like psychosis: A case report. *Am. J. Neuroradiol.* **26,** 2527–2529 (2005).

40. Oliveira, J. R. M. & Oliveira, M. F. Primary brain calcification in patients undergoing treatment with the biphosphanate alendronate. *Sci. Rep.* **6,** 22961 (2016).

41. Forster, I. C., Hernando, N., Biber, J. & Murer, H. Phosphate transporters of the SLC20 and SLC34 families. *Mol Asp. Med* **34,** 386–395 (2013).

42. Reimer, R. J. SLC17: A functionally diverse family of organic anion transporters. *Molecular Aspects of Medicine* **34,** 350–359 (2013).

43. Sabbagh, Y., Giral, H., Caldas, Y., Levi, M. & Schiavi, S. C. Intestinal Phosphate Transport. *Advances in Chronic Kidney Disease* **18,** 85–90 (2011).

44. Chavkin, N. W., Chia, J. J., Crouthamel, M. H. & Giachelli, C. M. Phosphate uptake-independent signaling functions of the type III sodium-dependent phosphate transporter, PiT-1, in vascular smooth muscle cells. *Exp. Cell Res.* **333,** 39–48 (2015).

45. Miller, D. G., Edwards, R. H. & Miller, A. D. Cloning of the cellular receptor for amphotropic murine retroviruses reveals homology to that for gibbon ape leukemia virus. *Proc. Natl. Acad. Sci. U. S. A.* **91,** 78–82 (1994).

46. O'Hara, B. *et al.* Characterization of a human gene conferring sensitivity to infection by gibbon ape leukemia virus. *Cell Growth Differ.* **1,** 119–27 (1990).

47. Kavanaugh, M. P. *et al.* Cell-surface receptors for gibbon ape leukemia virus and amphotropic murine retrovirus are inducible sodium-dependent phosphate symporters. *Proc. Natl. Acad. Sci.* **91 VN - r,** 7071–7075 (1994).

48. Olah, Z., Lehel, C., Anderson, W. B., Eiden, M. V. & Wilson, C. A. The cellular receptor for gibbon ape leukemia virus is a novel high affinity sodium-dependent phosphate transporter. *J. Biol. Chem.* **269,** 25426–25431 (1994).

49. Ravera, S., Virkki, L. V, Murer, H. & Forster, I. C. Deciphering PiT transport kinetics and substrate specificity using electrophysiology and flux measurements. *Am. J. Physiol. Cell Physiol.* **293,** C606–C620 (2007).

50. Bottger, P. & Pedersen, L. Mapping of the minimal inorganic phosphate transporting unit of human PiT2 suggests a structure universal to PiT-related proteins from all kingdoms of life. *BMC Biochem.* **12,** 21 (2011).

51. Farrell, K. B., Tusnady, G. E. & Eiden, M. V. New structural arrangement of the extracellular regions of the phosphate transporter SLC20A1, the receptor for gibbon ape leukemia virus. *J. Biol. Chem.* **284,** 29979–29987 (2009).

52. Salaün, C., Rodrigues, P. & Heard, J. M. Transmembrane topology of PiT-2, a phosphate transporter-retrovirus receptor. *J. Virol.* **75,** 5584–5592 (2001).

53. Feldman, S. A., Farrell, K. B., Murthy, R. K., Russ, J. L. & Eiden, M. V. Identification of an extracellular domain within the human PiT2 receptor that is required for amphotropic murine leukemia virus binding. *J. Virol.* **78,** 595–602 (2004).

54. Johann, S. V, van Zeijl, M., Cekleniak, J. & O'Hara, B. Definition of a domain of GLVR1 which is necessary for infection by gibbon ape leukemia virus and which is highly polymorphic between species. *J. Virol.* **67,** 6733–6736 (1993).

55. Festing, M. H., Speer, M. Y., Yang, H. Y. & Giachelli, C. M. Generation of mouse conditional and null alleles of the type III sodium-dependent phosphate cotransporter PiT-1. *Genesis* **47,** 858–863 (2009).

56. Beck, L. *et al.* The phosphate transporter PiT1 (Slc20a1) revealed as a new essential gene for mouse liver development. *PLoS One* **5,** (2010).

57. Li, X., Yang, H. Y. & Giachelli, C. M. Role of the sodium-dependent phosphate cotransporter, Pit-1, in vascular smooth muscle cell calcification. *Circ. Res.* **98,** 905–912 (2006).

58. Liu, L., Sanchez-Bonilla, M., Crouthamel, M., Giachelli, C. & Keel, S. Mice lacking the sodium-dependent phosphate import protein, PiT1 (SLC20A1), have a severe defect in

terminal erythroid differentiation and early B cell development. *Exp. Hematol.* **41,** 432–443 (2013).

59. Tatsumi, S. *et al.* Molecular cloning and hormonal regulation of PiT-1, a sodium-dependent phosphate cotransporter from rat parathyroid glands. *Endocrinology* **139,** 1692–1699 (1998).

60. Beck, L. *et al.* Identification of a novel function of PiT1 critical for cell proliferation and independent of its phosphate transport activity. *J. Biol. Chem.* **284,** 31363–31374 (2009).

61. Salaün, C. *et al.* Identification of a novel transport-independent function of PiT1/SLC20A1 in the regulation of TNF-induced apoptosis. *J. Biol. Chem.* **285,** 34408–34418 (2010).

62. Bottger, P. & Pedersen, L. Two highly conserved glutamate residues critical for type III sodium-dependent phosphate transport revealed by uncoupling transport function from retroviral receptor function. *J Biol Chem* **277,** 42741–42747 (2002).

63. Amann, K. Media calcification and intima calcification are distinct entities in chronic kidney disease. *Clin J Am Soc Nephrol* **3,** 1599–1605 (2008).

64. van der Wal, A. C. & Becker, A. E. Atherosclerotic plaque rupture--pathologic basis of plaque stability and instability. *Cardiovasc. Res.* **41,** 334–344 (1999).

65. Jablonski, K. L. & Chonchol, M. Vascular calcification in end-stage renal disease. *Hemodial Int* **17 Suppl 1,** S17–21 (2013).

66. Lusis, A. J. Atherosclerosis. *Nature* **407,** 233–241 (2000).

67. Farb, A. *et al.* Sudden coronary death. Frequency of active coronary lesions, inactive coronary lesions, and myocardial infarction. *Circulation* **92,** 1701–1709 (1995).

68. Pai, A. S. & Giachelli, C. M. Matrix remodeling in vascular calcification associated with chronic kidney disease. *J Am Soc Nephrol* **21,** 1637–1640 (2010).

69. Guerin, A. P., Pannier, B., Metivier, F., Marchais, S. J. & London, G. M. Assessment and significance of arterial stiffness in patients with chronic kidney disease. *Curr Opin Nephrol Hypertens* **17,** 635–641 (2008).

70. Nitta, K. *et al.* Left ventricular hypertrophy is associated with arterial stiffness and

vascular calcification in hemodialysis patients. *Hypertens Res* **27,** 47–52 (2004).

71. Shanahan, C. M. *et al.* Medial localization of mineralization-regulating proteins in association with Monckeberg's sclerosis: evidence for smooth muscle cell-mediated vascular calcification. *Circulation* **100,** 2168–2176 (1999).

72. Wu, M., Rementer, C. & Giachelli, C. M. Vascular calcification: An update on mechanisms and challenges in treatment. *Calcif. Tissue Int.* **93,** 365–373 (2013).

73. Rensen, S. S. M., Doevendans, P. A. F. M. & van Eys, G. J. J. M. Regulation and characteristics of vascular smooth muscle cell phenotypic diversity. *Neth. Heart J.* **15,** 100–8 (2007).

74. Shanahan, C. M., Cary, N. R., Metcalfe, J. C. & Weissberg, P. L. High expression of genes for calcification-regulating proteins in human atherosclerotic plaques. *J. Clin. Invest.* **93,** 2393–2402 (1994).

75. Tyson, K. L. *et al.* Osteo/chondrocytic transcription factors and their target genes exhibit distinct patterns of expression in human arterial calcification. *Arterioscler. Thromb. Vasc. Biol.* **23,** 489–494 (2003).

76. Steitz, S. A. *et al.* Smooth muscle cell phenotypic transition associated with calcification: upregulation of Cbfa1 and downregulation of smooth muscle lineage markers. *Circ. Res.* **89,** 1147–1154 (2001).

77. Tintut, Y. *et al.* Multilineage Potential of Cells from the Artery Wall. *Circulation* **108,** 2505–2510 (2003).

78. Iyemere, V. P., Proudfoot, D., Weissberg, P. L. & Shanahan, C. M. Vascular smooth muscle cell phenotypic plasticity and the regulation of vascular calcification. *Journal of Internal Medicine* **260,** 192–210 (2006).

79. Rutsch, F. *et al.* Mutations in ENPP1 are associated with 'idiopathic' infantile arterial calcification. *Nat. Genet.* **34,** 379–81 (2003).

80. Luo, G. *et al.* Spontaneous calcification of arteries and cartilage in mice lacking matrix GLA protein. *Nature* **386,** 78–81 (1997).

81. Bucay, N. *et al.* osteoprotegerin-deficient mice develop early onset osteoporosis and arterial calcification. *Genes Dev* **12,** 1260–1268 (1998).

82. Moe, S. M. *et al.* Role of calcification inhibitors in the pathogenesis of vascular calcification in chronic kidney disease (CKD). *Kidney Int.* **67,** 2295–2304 (2005).

83. Stenvinkel, P. *et al.* Low fetuin-A levels are associated with cardiovascular death: Impact of variations in the gene encoding fetuin. *Kidney Int.* **67,** 2383–2392 (2005).

84. Giachelli, C. M. *et al.* Osteopontin is elevated during neointima formation in rat arteries and is a novel component of human atherosclerotic plaques. *J. Clin. Invest.* **92,** 1686–1696 (1993).

85. Jono, S., Peinado, C. & Giachelli, C. M. Phosphorylation of osteopontin is required for inhibition of vascular smooth muscle cell calcification. *J Biol Chem* **275,** 20197–20203 (2000).

86. Giachelli, C. M. Ectopic Calcification : Gathering Hard Facts about Soft Tissue Mineralization. *Am. J. Pathol.* **154,** 671–675 (1999).

87. Boström, K. *et al.* Bone morphogenetic protein expression in human atherosclerotic lesions. *J. Clin. Invest.* **91,** 1800–9 (1993).

88. Dhore, C. R. *et al.* Differential Expression of Bone Matrix Regulatory Proteins in Human Atherosclerotic Plaques. *Arterioscler. Thromb. Vasc. Biol.* **21,** 1998–2003 (2001).

89. Schluesener, H. J. & Meyermann, R. Immunolocalization of BMP-6, a novel TGF-ß-related cytokine, in normal and atherosclerotic smooth muscle cells. *Atherosclerosis* **113,** 153–156 (1995).

90. Hirota, S. *et al.* Expression of osteopontin messenger RNA by macrophages in atherosclerotic plaques. A possible association with calcification. *Am. J. Pathol.* **143,** 1003–1008 (1993).

91. O'Brien, K. D. *et al.* Osteopontin is expressed in human aortic valvular lesions. *Circulation* **92,** 2163–8 (1995).

92. Ikeda, T., Shirasawa, T., Esaki, Y., Yoshiki, S. & Hirokawa, K. Osteopontin mRNA is expressed by smooth muscle-derived foam cells in human atherosclerotic lesions of the aorta. *J. Clin. Invest.* **92,** 2814–2820 (1993).

93. Fitzpatrick, L. A., Severson, A., Edwards, W. D. & Ingram, R. T. Diffuse calcification in human coronary arteries: Association of osteopontin with atherosclerosis. *J. Clin. Invest.* **94,** 1597–1604 (1994).

94. Shioi, A. *et al.* beta-Glycerophosphate Accelerates Calcification in Cultured Bovine Vascular Smooth Muscle Cells. *Arterioscler. Thromb. Vasc. Biol.* **15,** 2003–2009 (1995).

95. Proudfoot, D., Skepper, J. N., Shanahan, C. M. & Weissberg, P. L. Calcification of human vascular cells in vitro is correlated with high levels of matrix Gla protein and low levels of osteopontin expression. *Arter. Thromb Vasc Biol* **18,** 379–388 (1998).

96. Alves, R. D. A. M., Eijken, M., van de Peppel, J. & van Leeuwen, J. P. T. M. Calcifying vascular smooth muscle cells and osteoblasts: independent cell types exhibiting extracellular matrix and biomineralization-related mimicries. *BMC Genomics* **15,** 965 (2014).

97. Panizo, S. *et al.* RANKL increases vascular smooth muscle cell calcification through a rank-bmp4-dependent pathway. *Circ. Res.* **104,** 1041–1048 (2009).

98. Callegari, A., Coons, M. L., Ricks, J. L., Rosenfeld, M. E. & Scatena, M. Increased calcification in osteoprotegerin-deficient smooth muscle cells: Dependence on receptor activator of NF-κB ligand and interleukin 6. *J. Vasc. Res.* **51,** 118–31 (2014).

99. Ewence, A. E. *et al.* Calcium phosphate crystals induce cell death in human vascular smooth muscle cells: A potential mechanism in atherosclerotic plaque destabilization. *Circ. Res.* **103,** (2008).

100. Anderson, H. C. Matrix vesicles and calcification. *Curr. Rheumatol. Rep.* **5,** 222–226 (2003).

101. Tanimura, A., McGregor, D. H. & Anderson, H. C. Matrix vesicles in atherosclerotic calcification. *Proc. Soc. Exp. Biol. Med.* **172,** 173–7 (1983).

102. Proudfoot, D. *et al.* Apoptosis regulates human vascular calcification in vitro: evidence for initiation of vascular calcification by apoptotic bodies. *Circ. Res.* **87,** 1055–1062 (2000).

103. Bentzon, J. F., Otsuka, F., Virmani, R. & Falk, E. Mechanisms of plaque formation and rupture. *Circ. Res.* **114,** 1852–1866 (2014).

104. Smith, E. R. *et al.* Elastin degradation is associated with progressive aortic stiffening and all-cause mortality in predialysis chronic kidney disease. *Hypertension* **59,** 973–978 (2012).

105. Pai, A., Leaf, E. M., El-Abbadi, M. & Giachelli, C. M. Elastin degradation and vascular smooth muscle cell phenotype change precede cell loss and arterial medial calcification in a uremic mouse model of chronic kidney disease. *Am J Pathol* **178,** 764–773 (2011).

106. Vyavahare, N., Jones, P. L., Tallapragada, S. & Levy, R. J. Inhibition of matrix metalloproteinase activity attenuates tenascin-C production and calcification of implanted purified elastin in rats. *Am. J. Pathol.* **157,** 885–93 (2000).

107. Rucker, R. B. Calcium binding to elastin. *Adv. Exp. Med. Biol.* **48,** 185–209 (1974).

108. Ichikawa, S. *et al.* A homozygous missense mutation in human KLOTHO causes severe tumoral calcinosis. *J. Clin. Invest.* **117,** 2684–2691 (2007).

109. Chefetz, I. *et al.* GALNT3, a gene associated with hyperphosphatemic familial tumoral calcinosis, is transcriptionally regulated by extracellular phosphate and modulates matrix metalloproteinase activity. *Biochim. Biophys. Acta - Mol. Basis Dis.* **1792,** 61–67 (2009).

110. Benet-Pagès, A., Orlik, P., Strom, T. M. & Lorenz-Depiereux, B. An FGF23 missense mutation causes familial tumoral calcinosis with hyperphosphatemia. *Hum. Mol. Genet.* **14,** 385–390 (2005).

111. Block, G. A. Prevalence and clinical consequences of elevated Ca x P product in hemodialysis patients. *Clin Nephrol* **54,** 318–324 (2000).

112. El-Abbadi, M. M. *et al.* Phosphate feeding induces arterial medial calcification in uremic mice: role of serum phosphorus, fibroblast growth factor-23, and osteopontin. *Kidney Int* **75,** 1297–1307 (2009).

113. Lau, W. L. *et al.* High phosphate feeding promotes mineral and bone abnormalities in mice with chronic kidney disease. *Nephrol Dial Transpl.* **28,** 62–69 (2013).

114. Shanahan, C. M., Crouthamel, M. H., Kapustin, A. & Giachelli, C. M. Arterial calcification in chronic kidney disease: key roles for calcium and phosphate. *Circ. Res.* **109,** 697–711 (2011).

115. Adeney, K. L. *et al.* Association of serum phosphate with vascular and valvular calcification in moderate CKD. *J Am Soc Nephrol* **20,** 381–387 (2009).

116. Block, G., Hulbert-Shearon, T., Levin, N. & Port, F. Association of serum phosphorus and calcium x phosphate product with mortality risk in chronic hemodialysis patients: A national study. *Am. J. Kidney Dis.* **31,** 607–617 (1998).

117. Autier, P. & Gandini, S. Vitamin D supplementation and total mortality: a meta-analysis of randomized controlled trials. *Arch. Intern. Med.* **167,** 1730–7 (2007).

118. St Peter, W. L. *et al.* Effects of monthly dose and regular dosing of intravenous active vitamin D use on mortality among patients undergoing hemodialysis. *Pharmacotherapy* **29,** 154–164 (2009).

119. Goldsmith, D. J., Covic, A., Sambrook, P. A. & Ackrill, P. Vascular calcification in long-term haemodialysis patients in a single unit: a retrospective analysis. *Nephron* **77,** 37–43 (1997).

120. Bas, A., Lopez, I., Perez, J., Rodriguez, M. & Aguilera-Tejero, E. Reversibility of calcitriol-induced medial artery calcification in rats with intact renal function. *J. Bone Miner. Res.* **21,** 484–90 (2006).

121. Haffner, D. *et al.* Systemic cardiovascular disease in uremic rats induced by 1,25(OH)2D3. *J. Hypertens.* **23,** 1067–75 (2005).

122. Block, G. a *et al.* Mineral metabolism, mortality, and morbidity in maintenance hemodialysis. *J. Am. Soc. Nephrol.* **15,** 2208–2218 (2004).

123. London, G. M. *et al.* Arterial calcifications and bone histomorphometry in end-stage renal disease. *J. Am. Soc. Nephrol.* **15,** 1943–1951 (2004).

124. Coen, G. *et al.* Are PTH serum levels predictive of coronary calcifications in haemodialysis patients? *Nephrol. Dial. Transplant.* **22,** 3262–3267 (2007).

125. Hamilton, D. L. & Abremski, K. Site-specific recombination by the bacteriophage P1 lox-Cre system. Cre-mediated synapsis of two lox sites. *J. Mol. Biol.* **178,** 481–486 (1984).

126. Nagy, A. Cre recombinase: the universal reagent for genome tailoring. *Genesis* **26,** 99–109 (2000).

127. Voziyanov, Y., Pathania, S. & Jayaram, M. A general model for site-specific recombination by the integrase family recombinases. *Nucleic Acids Res.* **27,** 930–941 (1999).

128. Jono, S. *et al.* Phosphate regulation of vascular smooth muscle cell calcification. *Circ. Res.* **87,** E10–7 (2000).

129. Prosdocimo, D. a, Douglas, D. C., Romani, A. M., O'Neill, W. C. & Dubyak, G. R. Autocrine ATP release coupled to extracellular pyrophosphate accumulation in vascular smooth muscle cells. *Am. J. Physiol. Cell Physiol.* **296,** C828–C839 (2009).

130. Trapnell, C. *et al.* Transcript assembly and quantification by RNA-Seq reveals unannotated transcripts and isoform switching during cell differentiation. *Nat. Biotechnol.* **28,** 511–515 (2010).

131. Trapnell, C. *et al.* Differential analysis of gene regulation at transcript resolution with RNA-seq. *Nat. Biotechnol.* **31,** 46–53 (2013).

132. Liu, L. & Duff, K. A technique for serial collection of cerebrospinal fluid from the cisterna magna in mouse. *J. Vis. Exp. JoVE* **21,** 10–12 (2008).

133. Guerreiro, P. M., Bataille, A. M., Parker, S. L. & Renfro, J. L. Active removal of inorganic phosphate from cerebrospinal fluid by the choroid plexus. *Am. J. Physiol. Renal Physiol.* **306,** F1275–84 (2014).

134. Bornfeldt, K. E. *et al.* Insulin-like growth factor-I and platelet-derived growth factor-BB induce directed migration of human arterial smooth muscle cells via signaling pathways that are distinct from those of proliferation. *J. Clin. Invest.* **93,** 1266–1274 (1994).

135. Hellström, M., Kalén, M., Lindahl, P., Abramsson, A. & Betsholtz, C. Role of PDGF-B and PDGFR-β in recruitment of vascular smooth muscle cells and pericytes during embryonic blood vessel formation in the mouse. *Development* **126,** 3047–3055 (1999).

136. Bornfeldt, K. E. *et al.* Sphingosine-1-phosphate inhibits PDGF-induced chemotaxis of human arterial smooth muscle cells: spatial and temporal modulation of PDGF chemotactic signal transduction. *J. Cell Biol.* **130,** 193–206 (1995).

137. Okura, T. *et al.* Platelet-derived growth factor induces apoptosis in vascular smooth muscle cells: roles of the Bcl-2 family. *Biochim. Biophys. Acta* **1403,** 245–53 (1998).

138. Demoulin, J.-B. *et al.* Platelet-derived growth factor stimulates membrane lipid synthesis through activation of phosphatidylinositol 3-kinase and sterol regulatory element-binding proteins. *J. Biol. Chem.* **279,** 35392–35402 (2004).

139. Holmsen, H., Male, R., Rongved, S., Langeland, N. & Lillehaug, J. Platelet-derived-growth-factor-stimulated heterogeneous polyphosphoinositide metabolism and phosphate uptake in C3H fibroblasts. *Biochem. J.* **260,** 589–592 (1989).

140. Zhen, X., Bonjour, J. P. & Caverzasio, J. Platelet-Derived Growth Factor Stimulates Sodium-Dependent Pi Transport in Osteoblastic Cells via Phospholipase Cγ and Phosphatidylinositol 3′-Kinase. *J. Bone Miner. Res.* **12,** 36–44 (1997).

141. Giachelli, C. M. *et al.* Vascular calcification and inorganic phosphate. *Am. J. Kidney Dis.* **38,** S34–S37 (2001).

142. Fernandes, I., Béliveau, R., Friedlander, G. & Silve, C. NaPO(4) cotransport type III (PiT1) expression in human embryonic kidney cells and regulation by PTH. *Am. J. Physiol.* **277,** F543–51 (1999).